JGR Planets

RESEARCH ARTICLE
10.1029/2024JE008351

†Deceased January 2023

Key Points:

- Comparison of trace gases and aerosol opacity between ACS on ExoMars TGO and MCS on MRO
- Low correlations between HCl and the opacities of dust or water ice, but very strong correlation with water vapor and the formation of ices
- HCl source and sink possibilities are discussed, concluding that frost activity may be the most likely possibility for both

Supporting Information:

Supporting Information may be found in the online version of this article.

Correspondence to:

K. S. Olsen,
Kevin.Olsen@physics.ox.ac.uk

Citation:

Olsen, K. S., Fedorova, A. A., Kass, D. M., Kleinböhl, A., Trokhimovskiy, A., Korablev, O. I., et al. (2024). Relationships between HCl, H_2O, aerosols, and temperature in the Martian atmosphere: 2. Quantitative correlations. *Journal of Geophysical Research: Planets*, *129*, e2024JE008351. https://doi.org/10.1029/2024JE008351

Received 21 FEB 2024
Accepted 26 JUL 2024

Author Contributions:

Conceptualization: K. S. Olsen, O. I. Korablev, F. Montmessin
Data curation: K. S. Olsen, A. A. Fedorova, D. M. Kass, A. Kleinböhl, A. Trokhimovskiy, L. Baggio, J. Alday, D. A. Belyaev, J. A. Holmes, A. Patrakeev, A. Shakun
Formal analysis: K. S. Olsen, A. A. Fedorova, A. Trokhimovskiy, L. Baggio, J. Alday, D. A. Belyaev, J. A. Holmes, J. P. Mason, P. M. Streeter, K. Rajendran, M. R. Patel

Relationships Between HCl, H_2O, Aerosols, and Temperature in the Martian Atmosphere: 2. Quantitative Correlations

K. S. Olsen[1,2], A. A. Fedorova[3], D. M. Kass[4], A. Kleinböhl[4], A. Trokhimovskiy[3], O. I. Korablev[3], F. Montmessin[5], F. Lefèvre[5], L. Baggio[5], J. Alday[2], D. A. Belyaev[3], J. A. Holmes[2], J. P. Mason[2], P. M. Streeter[2], K. Rajendran[2], M. R. Patel[2], A. Patrakeev[3], and A. Shakun[3,†]

[1]Department of Physics, University of Oxford, Oxford, UK, [2]School of Physical Sciences, The Open University, Milton Keynes, UK, [3]Space Research Institute (IKI), Moscow, Russia, [4]Jet Propulsion Laboratory (JPL), California Institute of Technology, Pasadena, CA, USA, [5]Laboratoire Atmosphères, Milieux, Observations Spatiales (LATMOS/CNRS), Paris, France

Abstract The detection of hydrogen chloride (HCl) in the atmosphere of Mars was among the primary objectives of the ExoMars Trace Gas Orbiter (TGO) mission. Its discovery using the Atmospheric Chemistry Suite mid-infrared channel (ACS MIR) showed a distinct seasonality and possible link to dust activity. This paper is part 2 of a study investigating the link between HCl and aerosols by comparing gas measurements made with TGO to dust and water ice opacities measured with the Mars Climate Sounder (MCS). In part 1, we showed, and compared, the seasonal evolution of vertical profiles of HCl, water vapor, temperature, dust opacity, and water ice opacity over the dusty periods around perihelion (solar longitudes 180°–360°) across Mars years 34–36. In part 2, we investigated the quantitative correlations in the vertical distribution between each quantity, as well as ozone. We show that there is a strong positive correlation between HCl and water vapor, which is expected due to fast photochemical production rates for HCl when reacting with water vapor photolysis products. We also show a strong positive correlation between water vapor and temperature, but are unable to show any correlation between temperature and HCl. There are weak correlations between the opacities of dust and water ice, and dust and water vapor, but only very low correlations between dust and HCl. We close with a discussion of possible sources and sinks and that interactions between HCl and water ice are the most likely for both, given the inter-comparison.

Plain Language Summary The ExoMars Trace Gas Orbiter (TGO) has observed three Martian dusty seasons (summer in the southern hemisphere). In mid-2018, we made the first detection of hydrogen chloride (HCl) in the Martian atmosphere using the Atmospheric Chemistry Suite (ACS). Finding this gas, among others, was a priority of ExoMars because its primary source may be volcanic. Since then, we have observed two more dusty periods with the reappearance of HCl each time. In part 1, we presented the climatology of HCl over these three dusty periods (in Mars years 34, 35, and 36) and investigate their relationships with temperature and water vapor measured by ACS, and with airborne dust and water ice measured with the Mars Climate Sounder (MCS) on the Mars Reconnaissance Orbiter (MRO). In this paper, part 2, we quantify the correlations between HCl, water vapor, ozone, dust, temperature, and water ice. We show that HCl is closely correlated to water vapor, which is, in turn, correlated to temperature. There is only a very low correlation between HCl and dust or water ice, which both impact water vapor. Possible mechanisms for seasonal HCl production and destruction are discussed, concluding that the freeze-thaw cycle of atmospheric water is most likely.

1. Introduction

This is part 2 of a two-part series investigating the nature of HCl in the Martian atmosphere. HCl was detected for the first time in solar occultation spectra recorded with the ExoMars Trace Gas Orbiter (TGO) Atmospheric Chemistry Suite mid-infrared channel (ACS MIR) (Korablev et al., 2021). Detecting HCl was part of the primary objective of the TGO mission since it may be linked with active volcanic activity, which is a major source of atmospheric HCl on Earth (Graedel & Keene, 1995; Keene et al., 1999). The ACS MIR observations revealed a correlation with water vapor and a distinct seasonality coincident with dust activity, leading to a proposed

Funding acquisition: K. S. Olsen, O. I. Korablev, F. Montmessin, J. P. Mason, M. R. Patel
Investigation: K. S. Olsen, A. A. Fedorova, A. Trokhimovskiy, F. Lefèvre, J. Alday, D. A. Belyaev, J. A. Holmes, J. P. Mason, P. M. Streeter, K. Rajendran, M. R. Patel
Methodology: K. S. Olsen, A. Trokhimovskiy, F. Lefèvre
Project administration: K. S. Olsen, O. I. Korablev, F. Montmessin, J. P. Mason, M. R. Patel
Resources: K. S. Olsen, A. A. Fedorova, D. M. Kass, A. Kleinböhl, A. Trokhimovskiy, O. I. Korablev, F. Montmessin, L. Baggio, M. R. Patel, A. Patrakeev, A. Shakun
Software: K. S. Olsen
Supervision: K. S. Olsen, J. P. Mason, M. R. Patel
Validation: K. S. Olsen, A. A. Fedorova, A. Kleinböhl, A. Trokhimovskiy, F. Lefèvre, J. Alday, D. A. Belyaev, J. A. Holmes, P. M. Streeter, K. Rajendran, M. R. Patel
Visualization: K. S. Olsen
Writing – original draft: K. S. Olsen
Writing – review & editing: K. S. Olsen, A. A. Fedorova, A. Kleinböhl, A. Trokhimovskiy, F. Lefèvre, L. Baggio, J. Alday, J. A. Holmes, J. P. Mason, P. M. Streeter, K. Rajendran, M. R. Patel

possible link between HCl formation and dust activity (Korablev et al., 2021; Olsen, Trokhimovskiy, et al., 2021). Herein, we investigate the possible link between HCl abundances and the aerosol opacities of dust and water ice as measured by the Mars Climate Sounder (MCS) in co-located observations (Kleinböhl et al., 2009, 2017, 2020).

In part 1 (Olsen et al., 2024b), we presented three Mars years (MYs) of measurements of HCl volume mixing ratio (VMR) vertical profiles made using ACS MIR. Observations were presented between solar longitude (L_s) 180° and 360°, when it is spring and summer in the southern hemisphere and atmospheric dust loading is highest (we refer to this time frame as the perihelion period). We also presented simultaneous observations of water vapor measured with ACS MIR and the ACS near-infrared channel (ACS NIR), temperatures measured with ACS NIR and MCS, and the dust opacity and water ice opacity measured with MCS. The climatology of each quantity was described in detail, revealing how the lifting of dust (Figure 5 in Olsen et al., 2024b) causes temperatures to increase substantially at all altitudes where dust is present (Figure 6 in Olsen et al., 2024b). This also drives water vapor upward as the lower atmosphere expands (Figure 8 in Olsen et al., 2024b). The altitude of the hygropause rises to the height of significant dust activity, where a sharp temperature gradient limits the presence of water vapor above the dust, which can be seen in the water ice opacity measurements that outline the altitudes in which water vapor and dust are present (although water ice and vapor co-exist (Poncin et al., 2022)). The HCl VMRs follow those of the water vapor closely, being present over the same altitude ranges over the same time periods, having a higher abundance in the southern hemisphere than in the north, and featuring coincident increases in abundance (Figure 3 in Olsen et al., 2024b).

Here, in part 2, we present a quantitative inter-comparison between all the variables presented, as well as ozone (O_3) which is also measured with ACS MIR (Olsen et al., 2020). Pearson correlation coefficients were computed between every quantity investigated, as well as ancillary data, and correlation plots between HCl and the other gases and aerosols are presented in the following sections. We show, once again, that there is a strong correlation between H_2O and HCl, which is expected since the fastest photochemical reaction to form HCl is via the photolysis byproducts of water vapor (e.g., Catling et al., 2010). What we seek to understand is what is the reservoir of active chlorine by which such a reaction can take place? We conclude with a discussion of several possible source and sink mechanisms for HCl, their support in literature, and their likelihood, given our results.

For each ACS MIR observation in which we are able to detect HCl, we also retrieve water vapor VMR. Simultaneous observations of the same air mass are made using ACS NIR, which provides measurements of water vapor VMR and temperature. See part 1 for details about each instrument, retrieval, and data set (Olsen et al., 2024b). The retrieved vertical profiles from ACS MIR and ACS NIR observations are on unique tangent height grids. In case there were errors made in the independent computations of the ACS MIR and ACS NIR tangent heights, which would introduce systematic biases, both data sets are interpolated to a uniform pressure grid. They are then directly compared to examine how these quantities depend on one another as they change over their vertical ranges. Since the frequency with which ACS NIR and ACS MIR acquire spectra is the same (2 s) and the viewing geometry is identical, both instruments have the same vertical resolutions.

For each ACS solar occultation, a co-located measurement may be found in the MCS data (within ±0.125° L_s and <500 km; see part 1 for methods; Olsen et al., 2024b). In general, several MCS observations can be found for each ACS solar occultation. We have performed the following investigation using the ensemble of MCS observations, the single closest MCS observation in time and space (minimizing the sum of normalized difference in distance and L_s), and the mean of the MCS profiles. We obtained similar correlation coefficients for each case, with some small variation. We present results using the mean MCS profile. There is variability within the MCS data set, and this provides the best estimate for state of the coincident air mass. Using the ensemble of data leads to biases toward those ACS MIR observations with many co-located MCS observations. The MCS data are interpolated to the uniform 1 km retrieval grid used for ACS MIR analysis, and the ACS MIR and MCS data are directly compared over their vertical ranges. This is sufficient to do without additional smoothing since ACS MIR and MCS have approximately the same vertical resolutions. Tangent height spacing for ACS MIR varies between 1 and 3.5 km, while MCS data have a vertical resolution of 5 km.

2. Results

Our results are summarized in Figure 1 which is a correlation table of all the quantities considered in this study: HCl, H_2O, and O_3 VMRs measured using ACS MIR, H_2O VMRs and temperatures measured using ACS NIR, the opacities of dust and water ice aerosols measured with MCS, and the latitude, longitude, tangent height (Z), L_s,

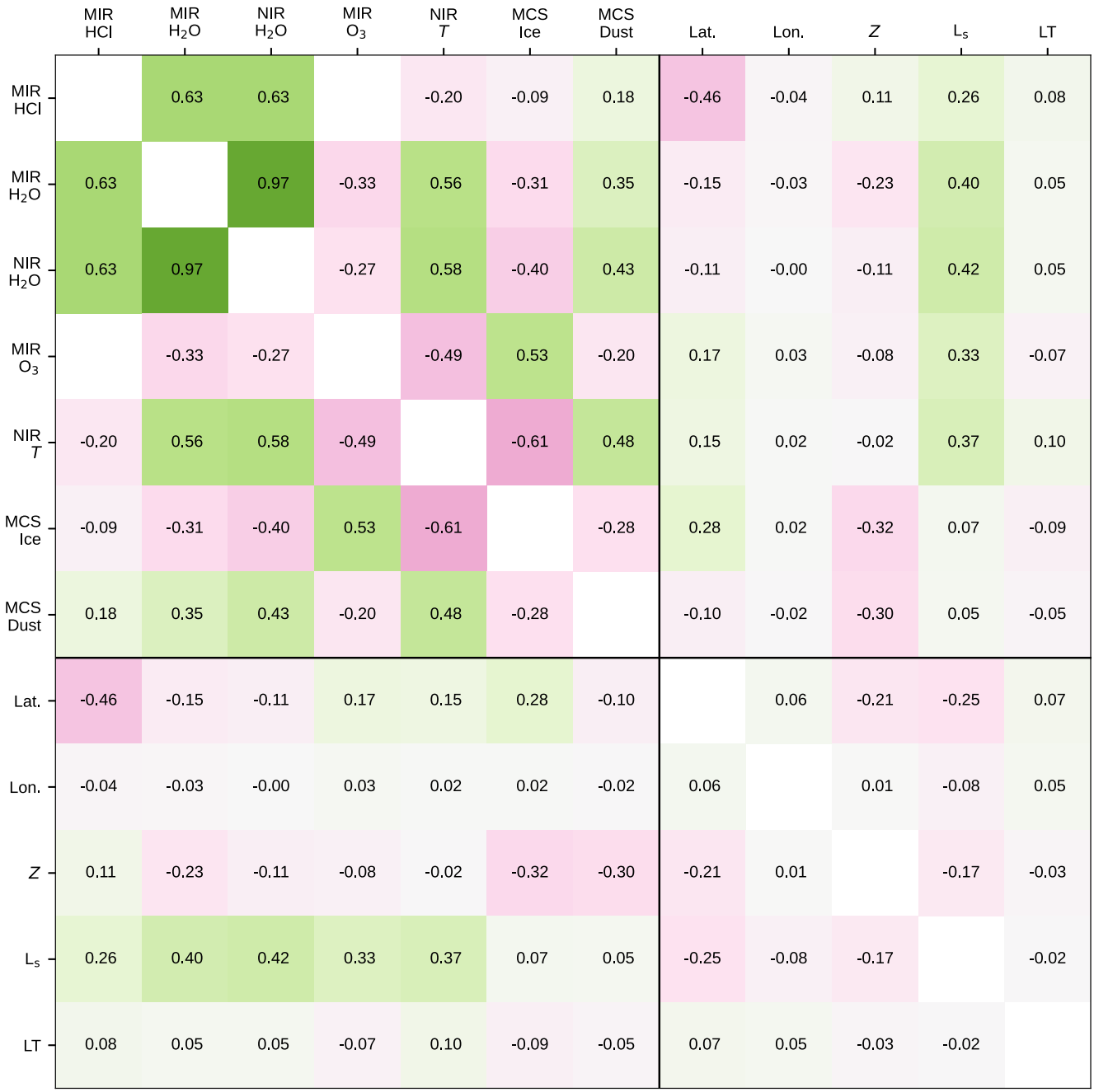

Figure 1. Correlation table for HCl VMR comparisons. This table shows the Pearson correlation coefficients between each different quantity included in this study computed between the ensemble of matched vertical profiles of simultaneous or coincident measurements. Colors correspond to the correlation magnitude, with green hues indicating positive correlations and purple hues indicating anti-correlations. Data is restricted to when HCl is observable: generally below 35 km and over the solar longitudes corresponding to southern spring and summer (see text).

and local time (LT). The ancillary data are included to ensure that observational biases are not being introduced without consideration. The latitude of the ACS solar occultation opportunities varies smoothly over L_s, which both limits the observational coverage of the ACS data, and introduces some observational biases. In both HCl and H_2O we find a low anti-correlation with latitude, which is expected since we observed higher VMRs of both gases in the southern hemisphere during southern summer (see part 1; Korablev et al., 2021; Olsen, Trokhimovskiy, et al., 2021; Fedorova et al., 2020; Fedorova et al., 2023; Olsen et al., 2024b). We see very low positive correlations with L_s which is explained by the maximum VMRs being found in the later part of the perihelion

period. Water ice opacity, water vapor VMR and dust opacity all have a weak anti-correlation with height, which indicates that their magnitudes generally all fall off at higher altitudes, which is again in agreement with their respective observations.

The data in Figure 1 convey overall trends within the data set, indicated with colors, but the values presented depend on the specific data provided and are expected to change a small amount over time and the growth of the ACS MIR data. They will also vary if restrictions are imposed, and these are shown and discussed in several places. For example, variations will occur over different latitude bands or altitude ranges. For our discussion, we define low or weak correlations as those with magnitudes <0.2, moderate correlations as between 0.2 and 0.45, and a strong correlation as >0.45.

As shown in Figure 1, we find a strong positive correlation (0.63) between the VMRs of water vapor and HCl along the vertical, and we find this to hold when comparing against the data products from either ACS MIR and ACS NIR. The water vapor retrievals from the two instruments are almost perfectly correlated, indicating that both instruments are consistent, and providing a layer of validation (we have also verified that there is no bias in the mean differences between the two). This is an encouraging result because the water vapor absorption features available within the spectral ranges resulting from using the ACS MIR secondary diffraction grating positions 11 and 12 are much weaker than those used by ACS NIR, limiting the sensitivity of ACS MIR and the altitude range over which retrievals can be performed.

We find a strong positive correlation between water vapor (ACS MIR and ACS NIR) and temperature (0.56, 0.58). Rather than indicating an increase in the water vapor abundance with rising atmospheric temperatures, this shows the removal of water vapor from different altitudes as the temperature falls off and water vapor condenses. Despite the strong correlation between HCl and H_2O, and between H_2O and T, we only find a moderate correlation between HCl and temperature (0.20).

In this study, we also introduced ozone which is measured using the position 12 configuration of ACS MIR (Olsen et al., 2020) and was recently compared to water vapor and temperature along the vertical in a similar fashion (Olsen et al., 2022). That study focused on southern fall and winter over which cold atmospheric temperatures lead to water vapor depletion, allowing for ozone to accumulate in the lower atmosphere. While there is limited temporal overlap in the HCl and O_3 measurements made with ACS MIR near the equinoctial periods, no observations were found that had overlapping quantities of both gases with sufficient confidence. We find a moderate anti-correlation between O_3 and H_2O (−0.33), and a strong anti-correlation with temperature (−0.49), consistent with our previous results in (Olsen et al., 2022). Because there is no overlap between HCl and O_3 detections, the ozone correlation data computed for Figure 1 is not restricted to the perihelion period. Therefore, the water vapor and temperature comparisons presented here are very similar to our prior work (Olsen et al., 2022). The anti-correlation between water vapor and ozone was expected due to their established photochemistry, and had been shown also for their vertical columns (Lefèvre et al., 2021), profiles (Patel et al., 2021), and had been explained using heterogeneous chemistry in a general circulation model (Brown et al., 2022).

What is surprising is the amount of variation in the ozone data relative to the water vapor, resulting in a low correlation coefficient relative to that between H_2O and HCl. This is indicative of the relative importance of water vapor in the photochemical production and loss of these species. The removal of odd-hydrogen (H and OH), traced by O_3 abundance, is controlled by HO_2, whose abundance is proportional to that of water vapor. However, the main source of O_3 is $O + O_2$, while its main loss process is photolysis. This cycle is neutral in terms of odd-oxygen (O and O_3), but the ozone abundance depends on those of O and O_2, and both O_3 and H_2O are highly variable. The relatively low correlation coefficient indicates a lack of equilibrium between atmospheric O_3 and H_2O. Furthermore, Olsen et al. (2022) showed that the overlapping altitude ranges of both gases were predominantly undergoing rapid changes over altitude, necessarily in opposite directions (e.g., H_2O VMR increasing with height while O_3 VMR falls), resulting in a reduction in the correlation coefficient.

Going further, we have compared ozone from ACS MIR with the aerosol opacities from MCS. We find that O_3 has a moderate anti-correlation with dust (−0.20; which leads to warmer temperatures and higher H_2O VMRs) and a strong correlation with ice (0.53; resulting from decreasing temperatures). The anti-correlation with temperature (−0.49) is stronger than with water vapor (−0.33), resulting in a stronger correlation with water ice (again, water ice and water vapor are strongly anti-correlated). Such relationships are already well established: Haider et al. (2022) identified relationships between dust loading and temperatures and the ozone abundance;

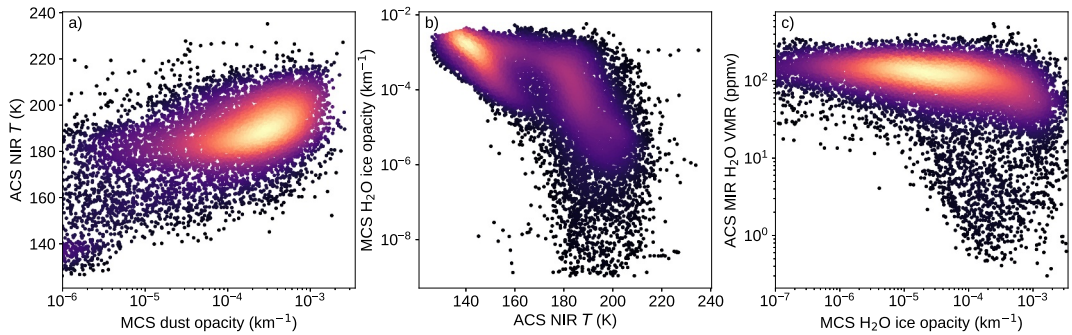

Figure 2. Parameter space for temperature, aerosols, and water vapor. Each panel shows a comparison between a collection of matched coincident vertical profiles, with each point a tangent height of an ACS solar occultation sequence. The comparisons shown in each panel are: (a) MCS dust opacities and ACS NIR temperatures; (b) ACS NIR temperatures and MCS ice opacities; and (c) MCS ice opacities and ACS MIR water vapor VMRs. Colors indicate the data density using a Gaussian kernel density estimate.

while Lefèvre et al. (2021) and Olsen et al. (2022) quantified the anti-correlation between water vapor and ozone using both total column and vertical profiles data sets. The strong positive correlation between water ice and ozone was expected due to the relationships of both to water vapor. Indirect evidence of this correlation comes from comparing the distributions of column average ozone observations (Clancy et al., 2016; Lefèvre et al., 2021; Mason et al., 2024) with those of water ice over the polar hoods during the fall and winter seasons (Giuranna et al., 2021; Olsen, Forget, et al., 2021; M. D. Smith, 2004, 2009), and a comparison is made by Holmes et al. (2018). The similarity in polar distributions is due to the formation of ice reducing water vapor abundance, allowing ozone to build. More direct evidence of this relationship comes from ozone vertical profile observations from equatorial regions around aphelion (Lebonnois et al., 2006; Olsen et al., 2022). These observations reveal the regular formation of an ozone layer above the aphelion cloud belt.

Temperature is also clearly linked to aerosols in the Martian atmosphere (e.g., Madeleine et al., 2011; Pollack et al., 1979; M. D. Smith et al., 2001). We find a strong correlation (0.48) between measured temperatures from ACS NIR and the dust opacity found with MCS. We also find a stronger anti-correlation (−0.61) between ACS NIR temperature measurements and MCS water ice opacities. These are shown in Figure 2, which illustrates the cascading effects that dust activity has on the Martian atmosphere. For relevance to the discussion of HCl, these correlations are restricted to heights <35 km where the strongest HCl absorption signatures are found. In (panel a) we show that increasing dust opacity leads to increasing temperatures, and in (panel b) we see that increasing temperatures reduce the water ice opacity, until temperatures become too warm to support any suspended ice in

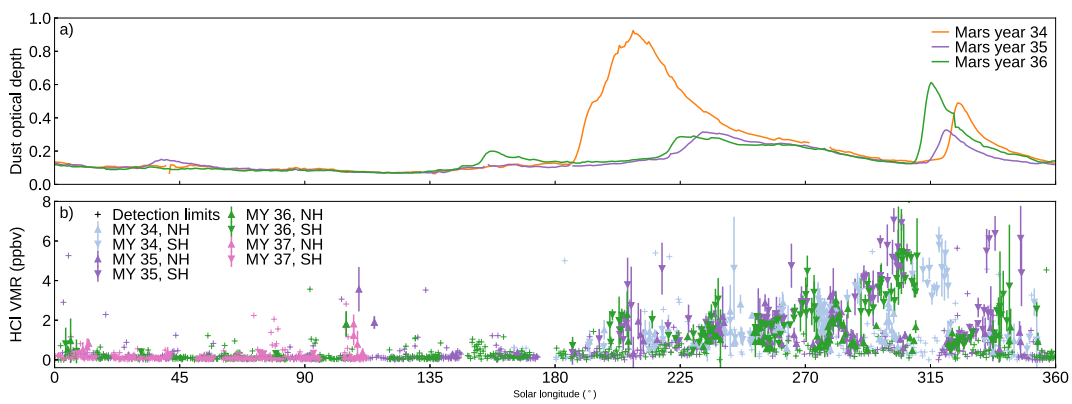

Figure 3. Timeline of HCl and dust activity. Panel (a) shows the globally averaged column dust optical depth from infrared absorption at 9.3 μm from Montabone et al. (2020) as a function of solar longitude (L_s) for Mars years 34–36. Panel (b) shows the maximum HCl VMR from each solar occultation vertical profile from ACS MIR. In the case where HCl was not detected, an upper limit is indicated with a plus symbol. Colors indicate Mars year and triangle direction indicates whether the observation was made in the northern hemisphere (NH; pointing up) or southern hemisphere (SH; pointing down).

the atmosphere. Of course, temperatures also impact water vapor, needed for ice formation, and (panel c) shows that as water ice opacity increases, we observe a corresponding decrease in water vapor VMR (anti-correlations of −0.31 and −0.40 for *T* from ACS MIR and ACS NIR, respectively). With these parameters, we also see that there is a threshold at which a maximum water ice content is observed with MCS (line-of-sight water ice becomes opaque) which is only reached when the water vapor VMR is depleted. That is, when there is substantial water vapor present in the lower atmosphere, >10–50 ppmv, the ice opacity always falls below this threshold. Thus we observe in Figure 2c an exclusion zone in the water vapor and ice parameter space where we do not observe low water ice opacities while the water vapor VMR is also low, and thin water ice layers are only associated with large amounts of water.

This study also demonstrates the impact that dust lifting has on the water ice, a result expected due to the associated warming caused by the dust, and described in part 1 (Olsen et al., 2024b). The measured anti-correlation between dust and water ice is −0.28, which follows the correlations with both parameters and temperature. The correlation between temperature and water ice opacity is −0.61, among the highest absolute value in Figure 1. Thus, we see that at all altitudes, dust loading directly leads to water ice depletion/sublimation.

The correlation coefficients computed between the VMR of HCl and the opacities of water ice and dust are low: −0.09 and 0.18, respectively. This tells us that while we observe HCl activity to be correlated to dust and water ice in time and vertical extent, the VMR of HCl does not strongly depend on the aerosol loading. These results are shown and discussed specifically in the following subsections.

2.1. Dust

One of the first, and most intriguing, characteristics of HCl in the Martian atmosphere that Korablev et al. (2021) and Olsen, Trokhimovskiy, et al. (2021) identified was that it was associated with the dusty season on Mars, appearing only after the onset of the 2018 global dust storm (GDS) and being reduced to below the low detection limits of the ACS MIR instrument during southern fall and winter seasons around aphelion. Figure 3 shows the seasonal changes of dust and HCl over three full MYs, from the start of ACS science operations until mid-MY 37. The upper panels show zonal means of the Martian dust climatologies derived from MCS observations by Montabone et al. (2020) for MYs 34–36. The lower panels show either the maximum HCl VMR for a given VMR vertical profile when HCl is detected with ACS MIR, or an upper limit when HCl was not detected. With very few exceptions, between $L_s = 0°$ and 180° only upper limits are shown (detections near $L_s = 110°$ were reported in Olsen, Trokhimovskiy, et al. (2021) and are addressed in Section 3). In all MYs, dust activity gradually begins to increase around the southern vernal equinox ($L_s = 180°$) until early season dust storms cause intense lifting. This follows the sublimation of the southern polar cap and the increase of atmospheric pressure. Regular regional dust storms begin by $L_s = 220°$ in MYs 35 and 36, but MY 34 is punctuated by the GDS at $L_s = 190°$, and MY 36 featured an unseasonal regional storm at $L_s = 165°$ (due to latitudinal constraints of ACS solar occultations, the area of this dust storm was not probed by ACS during that L_s period). In all MYs, dust abundances gradually decay after the early season storms until the late-season storms around $L_s = 315°$, after which the dust opacities again decay, but much quicker. The difference in the rate of change of dust opacities between around perihelion and the southern autumnal equinox is likely due to decreasing atmospheric pressure caused by the re-formation of the southern polar cap.

Likewise, in all MYs, we see a sudden increase in HCl detections and VMRs after $L_s = 180°$, coincident with dust lifting. By $L_s = 200°$, we are making regular detections of HCl with VMRs >1 ppmv in all MYs. Maximum VMRs are observed in the southern hemisphere just before the onset of the late-season dust storm. As we showed in part 1, these occur at lower altitudes and coincide with a falling hygropause (Olsen et al., 2024b) as the atmosphere cools and contracts after perihelion. At the end of southern summer, between $L_s = 330°$ and 360°, we observe a sudden and rapid decline in the HCl abundances and stop making detections at all after the southern autumnal equinox.

Because the variations in latitude over time of ACS MIR solar occultation opportunities were very similar in MYs 35 and 36 (see Figure 1 in part 1; Olsen et al., 2024b), we can clearly see hemispheric differences in Figure 3. Most of the variation in HCl abundance seen in Figure 3 is due to changes in latitude, such as the rapid increase observed in MYs 35 and 36 just after $L_s = 225°$, and followed by a gap in observations. This is a period where the solar occultations move from high northern and southern latitudes toward the equator. Strong differences between the HCl VMRs in the northern and southern hemisphere are visible around $L_s = 270°$, and again after $L_s = 285°$.

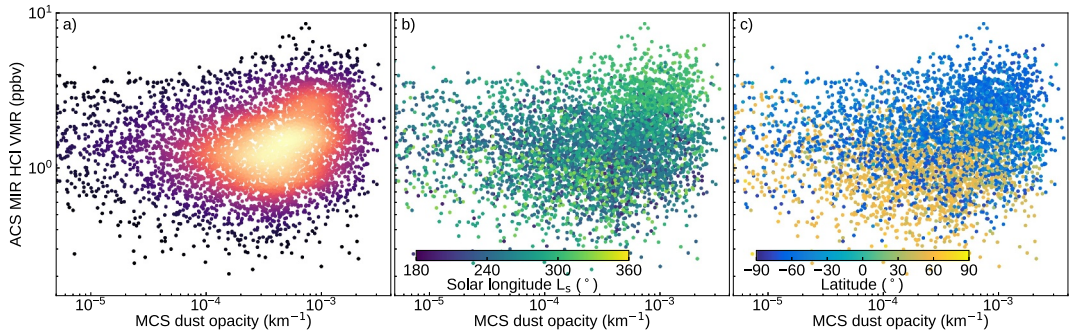

Figure 4. Parameter space between HCl VMR and dust opacity. Each panel shows a comparison between coincident measurements of MCS dust opacities and ACS MIR HCl VMRs. Each point represents a tangent height from an ACS MIR solar occultation sequence. The colors in each panel are: (a) data density using a Gaussian kernel estimate; (b) solar longitude (L_s); and (c) latitude.

The high northern latitudes have a low HCl abundance throughout the perihelion period of around 1 ppbv, while the southern hemisphere observations feature a growing HCl VMR from >2 ppbv after $L_s = 230°$ to 5–7 ppbv by $L_s = 300°$, just before the late-season storms.

Despite the temporal correlation between the start and end of seasonal dust activity and that of HCl, we find little evidence that the VMR of HCl depends on the amount of dust in the Martian atmosphere. Figure 4 shows the parameter space between dust opacity measured with MCS and the HCl VMR. Panel (a) shows the density of data (Gaussian kernel density estimate), (panel b) colors the data using L_s, and (panel c) colors the data using latitude. We see very little dependence on the time of the season (L_s), but note that higher HCl VMRs occur predominantly at southern latitudes which are also dustier. The correlation coefficient found was 0.18 indicating that there may be a general trend toward higher HCl VMRs occurring when dust opacities are higher (possibly driven by a cluster of high-VMR southern hemisphere observations in the upper-right corner of (panel c)), but this correlation has a very low magnitude. Chloride minerals are not uniformly distributed on the Martian surface, so if the chloride abundance within dust is nearly random, then this would be the expected correlation.

This is consistent with other attempts we have made to investigate a correlation with dust. For each solar occultation spectrum, the baseline transmittance is reduced by aerosol scattering which indicates the amount of dust loading in the atmosphere (Olsen, Trokhimovskiy, et al., 2021). No correlation is found between transmittance and HCl VMR. From the wide spectral range of the ACS thermal infrared channel, the dust abundance can be inferred from its absorption and scattering spectra, but coincident data are too sparse to reveal a correlation (Olsen, Trokhimovskiy, et al., 2021). We have also investigated the correlation between total dust optical depth, using the treatment of MCS data prepared by Montabone et al. (2020), but again, any correlation is very low.

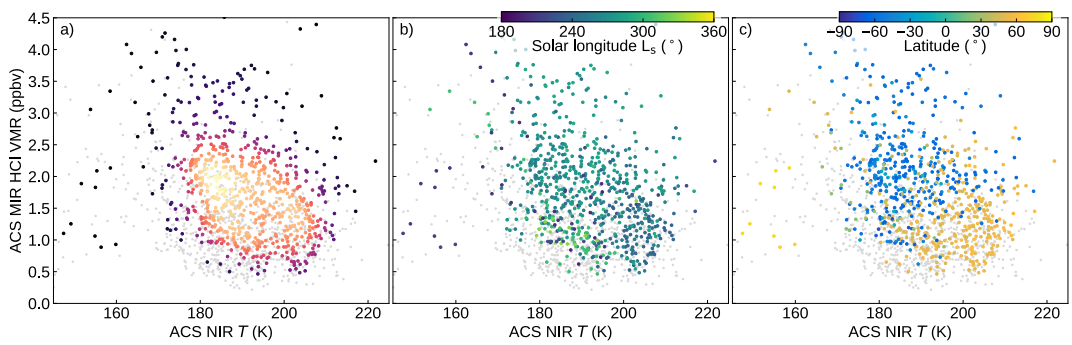

Figure 5. Parameter space between HCl VMR and temperature. Each panel shows a comparison between simultaneous measurements of ACS NIR temperatures and ACS MIR HCl VMRs. Each point represents a tangent height from an ACS MIR solar occultation sequence. The colors in each panel are: (a) data density using a Gaussian kernel estimate; (b) solar longitude (L_s); and (c) latitude. Data passing a 3σ selection rule for HCl are highlighted with colors, while gray data only pass a 2σ rule.

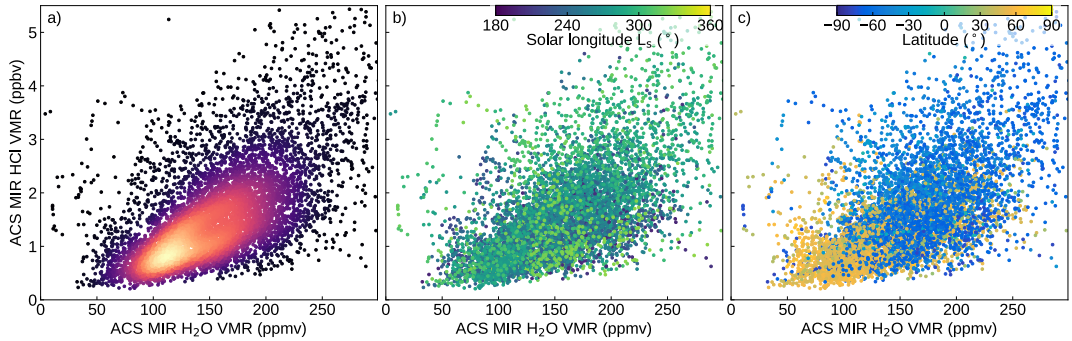

Figure 6. Parameter space between HCl and water vapor VMRs. Each panel shows a comparison between simultaneous measurements of the VMRs of H_2O and HCl from ACS MIR. Each point represents a tangent height from an ACS MIR solar occultation sequence. The colors in each panel are: (a) data density using a Gaussian kernel estimate; (b) solar longitude (L_s); and (c) latitude. A version of this figure using H_2O VMRs from ACS NIR is shown in the Supporting Information S1 (Figure S1).

2.2. Temperature

Due to the previously observed correlation between HCl and water vapor (Aoki et al., 2021; Korablev et al., 2021; Olsen, Trokhimovskiy, et al., 2021), which is strongly correlated with temperature (0.56 in Figure 1), a dependence on temperature for HCl was expected. However, when comparing vertical profiles of HCl VMR to simultaneously measured temperatures profiles from ACS NIR, we find only a low-to-moderate correlation along the vertical of −0.20. The parameter space between HCl VMRs from ACS MIR and the temperatures from ACS NIR is shown in Figure 5, with the density of the matched points given in panel a. There is little dependence on L_s (panel b), except that temperatures below 180 K occur more frequently toward the end of southern summer.

In Figure 5c we can see that while the highest HCl VMRs only occur at southern latitudes, but over a narrow range of temperature values, the coldest values for temperature are found at high northern latitudes and correspond to only low amounts of HCl. The warmest temperatures occur in the northern hemisphere for low amounts of HCl, and these data correspond to the MY 34 GDS. They occur at altitudes between 30 and 55 km over an L_s period of 215°–240°.

With HCl and temperature, we note a strong dependence on the altitude range of the ACS MIR data used, affected by varying the uncertainty-driven altitude selection rule for HCl. The vertical extent of retrieved VMRs is determined by their uncertainties, with VMRs greater than twice their uncertainty (2σ) shown (see part 1; Olsen et al., 2024b). This results in a correlation coefficient of −0.20, as given in Figure 1. However, if we strengthen the rule to 3σ, removing uncertain data from the upper and lower boundaries of the vertical profile, we obtain a correlation coefficient of −0.33. Reducing the rule to 1σ results in a coefficient of only −0.09. The colored data shown in Figure 5 use a 3σ rule, increasing the correlation coefficient, while additional data included using a 2σ rule is shown in gray.

The reason for this is the narrow altitude range over which we are able to measure HCl, which is difficult due to the weak signal. The temperature data used, inferred from strong CO_2 lines using the ACS NIR channel, is very stable with few variations over such a narrow altitude range. Thus, the correlation is negatively impacted by the variability of the HCl measurements compared to those of temperature.

2.3. Water Vapor

With the initial discovery of HCl in the Martian atmosphere, we noted a similarity between the shapes of the vertical profiles of water vapor and HCl VMRs (Korablev et al., 2021). After HCl reappeared a second time in MY 35, Olsen, Trokhimovskiy, et al. (2021) initially demonstrated a correlation between the VMRs of the two. Here, we reveal a strong correlation between the VMRs of H_2O and HCl over their vertical extent (0.63) using both ACS MIR secondary grating positions 11 and 12, three MYs of data, and much improved vertical sensitivity. This is shown in Figure 6, again showing the data density, dependence on L_s, and dependence on latitude. We can see that low abundances of HCl, <1 ppbv, predominantly occur when the VMR of H_2O is around 100 ppmv, and high abundances of HCl, >3 ppbv, tend to occur when the H_2O VMR is >200 ppmv, with very few measurements

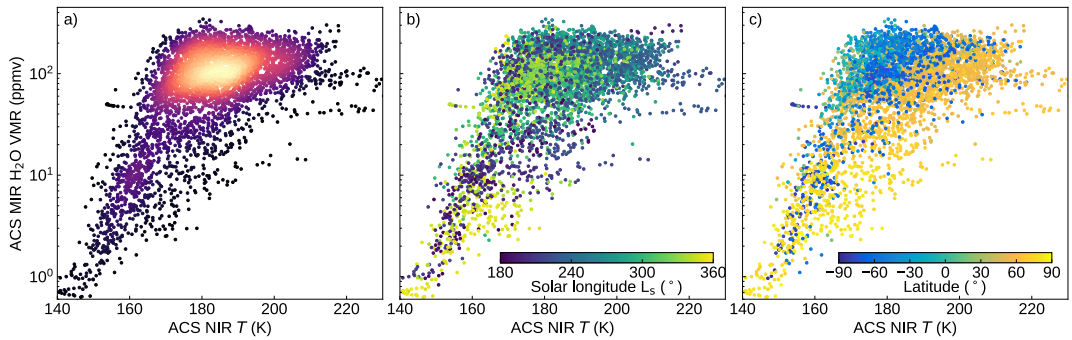

Figure 7. Parameter space between water vapor VMR and temperature. Each panel shows a comparison between simultaneous measurements of ACS NIR temperatures and ACS MIR HCl VMRs. Each point represents a tangent height from an ACS MIR solar occultation sequence. The colors in each panel are: (a) data density using a Gaussian kernel estimate; (b) solar longitude (L_s); and (c) latitude. A version of this figure using H_2O VMRs from ACS NIR is shown in the Supporting Information S1 (Figure S2).

made in the upper left areas of Figure 6a. There is a strong latitudinal dependence in Figure 6c, where the low-HCl and low-H_2O space is dominated by observations at northern latitudes (yellow), and the high-HCl and high-H_2O space is made up of southern hemisphere (blue) observations. A version of Figure 6 comparing ACS MIR HCl measurements with H_2O VMRs measured simultaneously using ACS NIR is given in Figure S1 of Supporting Information S1.

As shown by Olsen et al. (2022), there is a strong dependence of the H_2O VMR on temperature. Figure 7 shows the H_2O-temperature parameter space, shown again as Figure S2 in Supporting Information S1 using H_2O VMRs measured with ACS NIR. Between water vapor and temperature, we report a coefficient of 0.56 (0.58 using ACS NIR H_2O data). There are two clearly distinct groupings, corresponding to different hemisphere. At northern latitudes (yellow in Figure 7c), we have a broad range of temperatures that stretch from the warmest regions shown, to the coldest. As in the discussion of Figure 5, the warmest temperatures occurred between 30 and 55 km during the MY 34 GDS. The coldest values correspond to the norther winter, and this northern data set has consistently lower H_2O VMRs than in the south. The colder, low-H_2O data corresponds closely to that from the aphelion season and presented in Olsen et al. (2022) is shown in Figure S3 of Supporting Information S1 and discussed below.

The focus of Olsen et al. (2022) was on ozone that appears over the equinoxes and the aphelion period, and the parameter space and correlation found were for correspondingly low values of H_2O and a cold atmosphere. We only reported the correlation coefficient between the VMRs of O_3 and H_2O in Olsen et al. (2022), which were between −0.29 and −0.35. In Figure 1, we report a similar correlation coefficient between O_3 and H_2O of −0.33 (−0.27 using ACS NIR H_2O data). Differences can be largely attributed to the increasing size of the ACS MIR data set. To show that the current study is consistent with Olsen et al. (2022), Figure S3 in Supporting Information S1 shows the water vapor and temperature parameter space for the same L_s range as in Olsen et al. (2022), covering southern fall and winter. The correlation coefficient found is 0.56, consistent with the data covering southern spring and summer in Figure 7, despite differences in the structure of the parameter space (note the figures are shown with log scale on the *y*-axis, but the correlation coefficients are not computed as such - the correlation coefficient for the log of H_2O VMR and temperature increases over the aphelion period, in Figure S3 of Supporting Information S1, compared to the values in Figure 1, but does not significantly change for the data from southern spring and summer in Figure 7).

2.4. Water Ice

The correlation plot between HCl VMR and coincident measurements of water ice opacity from MCS (at 11.9 μm) is shown in Figure 8. As with the opacity of dust, the correlation along the vertical is low (−0.09), but indicates that water ice and HCl may be anti-correlated to some extent, whereas the correlation between dust and HCl was low and positive. Both results are consistent with the observed strong correlations between dust activity, temperature, and water vapor abundance. Despite these trends, however, we find that HCl VMRs between 0.5 and 5 ppbv occur over a very wide range of measured water ice opacities. The latitudinal information in Figure 8c

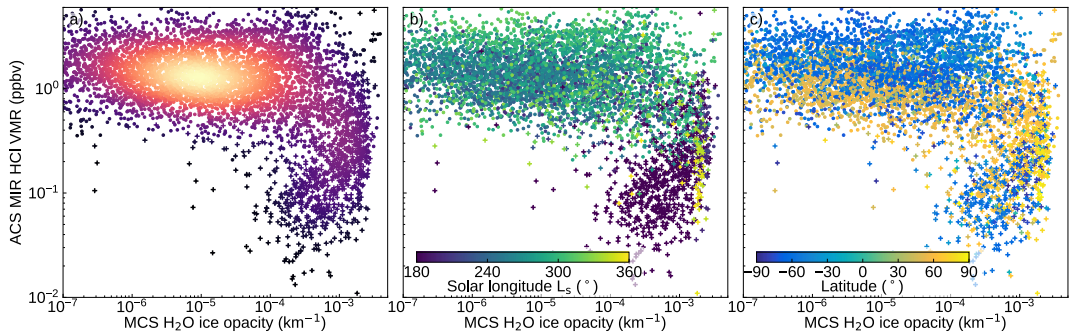

Figure 8. Parameter space between HCl VMR and ice opacity. Each panel shows a comparison between simultaneous measurements of MCS H_2O ice opacities and ACS MIR HCl VMRs. Each point represents a tangent height from an ACS MIR solar occultation sequence. The colors in each panel are: (a) data density using a Gaussian kernel estimate; (b) solar longitude (L_s); and (c) latitude.

indicates that the highest HCl VMRs occurred at southern latitudes, while the highest water ice opacities were found at northern latitudes.

Figure 8 also includes water ice data from over the aphelion period. Where an ACS MIR solar occultation was made, but no HCl detected, we have included the estimated upper limit, and the mean water ice opacity over the nominal HCl detection range (5–25 km). These are indicated with small crosses in the panels of Figure 8, and make up the data on the right-hand side of each panel. They are best distinguished in Figure 8b where their dark color indicates that they were predominantly obtained over an L_s range of 0°–180°. What we find is that HCl detections occur at all ice opacities, but predominantly below the 10^{-3} level. Conversely, non-detections only occur when the mean water ice opacity in the lower atmosphere approaches 10^{-3}. While the amount of water ice in the Martian atmosphere is not proportional to the HCl abundance, we can infer that there is an upper limit of ice opacity over which HCl will no longer be detected. Note that the lower-left area of Figure 8 remains empty when plotting the entire data set from ACS MIR (with its limitations). When the ice opacity falls below $<10^{-5}$, HCl becomes increasingly detectable with values >0.5 ppbv.

The shape occupied by the water ice and HCl parameter space in Figure 8 is very similar to that in Figure 2c, which compared water vapor to water ice. In both cases, a wide range of gas abundances for H_2O and HCl occur over the full range of measurable ice opacities, but once the ice reaches the 10^{-4}–10^{-3} range, the gas VMRs rapidly fall off. For water vapor, VMRs only fall below 10 ppmv when the ice opacity is high, while the HCl falls below its detectable level in the same water ice freezing conditions.

It must be noted that there is a maximum measurable ice opacity that MCS is sensitive to and, in some cases, measured data $>10^{-3}$ in Figure 8 may be representative of even greater ice loading in the atmosphere. There are also cases where the ice opacity may have been too high to retrieve accurately and these coincident data cannot be included in Figure 8. This maximum retrievable ice opacity accounts for the shapes of the parameter spaces shown in Figures 2c and 8.

2.5. Ozone

Ozone and HCl occur in opposite seasons due to their opposing relationships with water vapor. While we are unable to make a direct comparison of their VMRs along the vertical because of this, we have included ozone due to its known photochemical interactions with HCl. Terrestrially, HCl and the cycling of Cl between reservoirs, is responsible for catalytic cycles of ozone loss. The main pathway is the reaction $O_3 + Cl \rightarrow ClO + O_2$. On Earth, this forms the start of a catalytic cycle that reduces the abundance of odd-oxygen by converting O_3 into O_2, but remains neutral for Cl (von Glasow & Crutzen, 2003; X. Wang et al., 2019). In that case, ClO is converted into HOCl via reaction with HO_2, but over the aphelion period HO_2 abundances are strongly reduced by the condensation of water vapor, which is what allows ozone to build up. While the variations in both species are well explained by the seasonal changes in water vapor abundance, there is evidence that they should interact and enhance their observed anti-correlation.

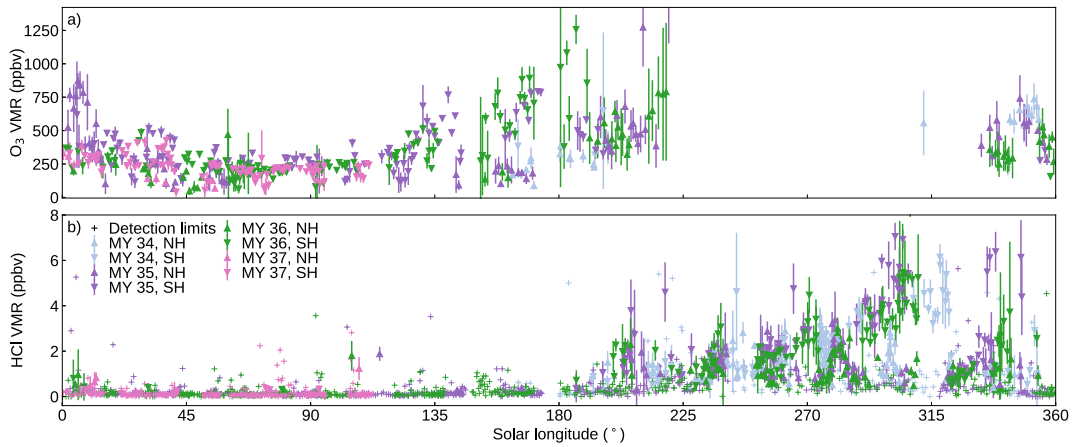

Figure 9. Timeline of HCl and ozone activity. Panel shows ACS MIR O_3 VMR measurements as a function of solar longitude (L_s) and panel (b) shows ACS MIR HCl VMR measurements over L_s, as in Figure 3. Each panel shows the maximum VMR of either O_3 or HCl from each solar occultation vertical profile recorded by ACS MIR. In the case where HCl was not detected, an upper limit is indicated with a plus symbol. Colors indicate Mars year and triangle direction indicates whether the observation was made in the northern hemisphere (NH; pointing up) or southern hemisphere (SH; pointing down).

Figure 9 shows the seasonal evolution of the ozone and HCl abundances over L_s. Panel a shows the maximum O_3 VMR in the lower atmosphere (<30 km) over MYs 34–37. There are enhancements toward the equinoxes, which is an observational phenomenon caused by the perpendicularity of Mars' rotational axis toward the sun. At these times, TGO solar occultations probe the furthest toward the poles where ozone is enhanced (see Figure 1 in part 1; Olsen et al., 2024b, 2022). During the aphelion period, while it is fall and winter in the southern hemisphere, ozone is allowed to build up and we observe ∼250 ppbv throughout. Conversely, while it is spring and summer in the south and the atmosphere contains 100–200 ppmv of water vapor up to 50–60 km, ozone is no longer detectable. This is diametrically opposite to our observations of HCl which were previously shown and discussed in Figure 3.

Two periods of interest are when ozone and HCl detections occur at the same time (though not simultaneously over the same altitudes and during the same occultation). Right after the southern vernal equinox, between $L_s = 180°$ and 220°, we observe a fall in the ozone abundances. This is partially related to the withdrawal of TGO solar occultation tangent points from the polar region, but also a strong response to the increasing warming and moistening of the Martian atmosphere. At the same time, we can see HCl abundances increasing.

Before the southern autumnal equinox, between $L_s = 320°$ and 360°, we observe the opposite behavior. Ozone abundances are increasing, while those of HCl sharply decline. While the behavior of both gases is controlled by atmospheric temperatures and water vapor abundances, and we do not simultaneously see measurable amounts of both gases simultaneously, their interactions have important implications for the aphelion period during which a permanent, boundary-layer reservoir of chlorine may be maintained cycling between Cl, HCl, and ClO.

The build up of ozone at this time may also be partially responsible for rapid destruction of HCl. Ozone is a good tracer for atomic oxygen (e.g., Lefèvre et al., 2021; Lefèvre & Krasnopolsky, 2017) since its primary destruction and production mechanisms are neutral in terms of odd-oxygen. Atomic oxygen may readily react with HCl to form either Cl or ClO via:

$$O + HCl \rightarrow OH + Cl.$$

Photochemical modeling work is required to determine the importance of this reaction and whether it can account for the rapid loss of HCl observed.

Krasnopolsky (2022) has shown that chlorine chemistry on Mars via O_3 + Cl and CO + Cl cycles is slower than the odd-hydrogen chemistry by orders of magnitude and weakly affects the basic photochemical products.

3. Discussion

While we have shown that HCl and water vapor are closely correlated and the photochemistry that governs HCl production from HO_2 is well known, the Cl source for that reaction is not understood, and neither is the rapid loss mechanism that occurs near the southern autumnal equinox. In this section, we provide a discussion of the possible HCl sources and sinks in the Martian atmosphere and their likelihood, given our observations with ACS. While the discussion follows the evidence of the correlations presented, we must reiterate that the specific values of the correlation coefficients may change as more data are collected, and depending on the specific constraints in the ranges of altitude, latitude, and L_s chosen.

3.1. Dust as a Source

Korablev et al. (2021) hypothesized a photochemical link between HCl and airborne dust fines. The basis for this was the likelihood that Martian dust may contain NaCl, and the established terrestrial photochemistry that forms tropospheric HCl from sea salt aerosols. Surface chlorides have been observed by the majority of Mars missions since Viking (Murchie et al., 2009; Osterloo et al., 2008; Ruesch et al., 2012), and from the Mars Exploration Rovers, we know that chloride minerals occur in airborne dust fines (Goetz et al., 2005). What remains unknown is the composition of those mineral chlorides. NaCl was identified in Martian meteorites (Bridges & Grady, 1999, 2000), while perchlorate was determined using the Phoenix lander (Hecht et al., 2009). Based on a comparison of hydrous mineral observations and those of chloride salts, Glotch et al. (2016) argue that NaCl is the most likely chloride salt observed from orbit and that is should be widespread. Chloride salts observed with Curiosity have also been interpreted to include NaCl (Thomas et al., 2019).

Terrestrially, airborne NaCl aerosols are a primary source of HCl in the troposphere (Graedel & Keene, 1995, 1996). Cl is volatilized by becoming hydrated and then oxidized, greatly aided by the uptake of the acids H_2SO_4 and HNO_3 (George & Abbatt, 2010; von Glasow & Crutzen, 2003). While there is a possibility that these acids are present in the atmosphere of Mars due to the presence of N_2 (M. L. Smith et al., 2014) and a history of volcanism, the relative abundance of nitrogen oxides (NO, NO_2, N_2O) and sulfur molecules (H_2S, SO_2, OCS) will be very low, since none of them have yet been detected in the Martian atmosphere (Braude et al., 2022; Maguire, 1977; Villanueva et al., 2013). Therefore, on Mars, the volatilization of Cl must be considered to be independent of the acid displacement step, which remains unproven. The alternative is via hydration to release free Cl^- ions for reactions on NaCl aerosol surfaces. Following the southern vernal equinox, the water vapor abundances are high enough for the necessary hydration to take place (Fedorova et al., 2020; Ladino & Abbatt, 2013; Santiago-Materese et al., 2018). Reactive chlorine in the salt aerosols may then readily react with HO_2 to form HCl. Additionally, Cl^- can heterogeneously react with OH to form Cl_2 (Knipping & Dabdub, 2002; Laskin et al., 2006; X. Wang et al., 2019). This will then photolyze to release gas-phase Cl radicals that may form HCl.

Aside from a photochemical mechanism to move Cl from dust aerosols into gas-phase molecules, there is evidence of several energetic processes that can separate Cl from chloride salts as well. Dust activity can turn over surface material and expose and lift aerosols that were previously protected from ultraviolet (UV) radiation. Solar UV may then be able to break down Cl-bearing aerosols, especially at higher altitudes (Carrier & Kounaves, 2015; Rao et al., 2012). High-energy cosmic radiation incident on the Martian surface may also be energetic enough to free chlorine ions of oxides into the atmosphere (Wilson et al., 2016). In this case, perchlorate on the surface or in the air may also be a source (Glavin et al., 2013; Quinn et al., 2013; Wilson et al., 2016).

Airborne dust activity will also stimulate electro-static discharges (Atreya et al., 2006) which have been shown to be able to also break down NaCl and other chloride salts (Martz'inez-Pabello et al., 2019; Rao et al., 2012; Wu et al., 2018). For Mars, the majority of work done to study surface chloride interactions has been in support of the formation of perchlorate, which generally follows the break-down of surface chloride salts, the volatilization of chlorine and chlorine oxides, and the subsequent formation of chlorate and perchlorate from HCl and ozone. More recently, experiments have been conducted to specifically investigate the production of HCl, rather than chlorate, via these processes. They have found that electro-static discharges may be able to account for observed HCl abundances, assuming a nominal discharge rate and distribution (A. Wang et al., 2020, 2023).

Since the discovery of HCl, photochemical modeling studies have been ongoing to investigate different dust-sourced pathways of HCl formation. Krasnopolsky (2022) developed a detailed model with production of HCl from heterogeneous reactions of $FeCl_3$ and NaCl with H and O and HCl loss on water ice. The model reproduced a

correlation between HCl and H_2O and seasonal differences in HCl abundance. The proposed reactions have not been confirmed by laboratory experiments or observed in nature, and their rates were chosen to fit the HCl observations. Taysum et al. (2024) examined a mechanism of the breakdown of hydrated perchlorate under incident UV radiation. While this result used realistic assumptions to obtain the abundances of HCl we have observed with ACS MIR, this mechanism is also not known to occur in nature and relies on limited laboratory work that remains unproven for Martian atmospheric conditions. Finally, Streeter et al. (2024) studied the impact of heterogeneous chlorine chemistry in a global climate model, building on the gas-phase chlorine chemistry scheme of Rajendran et al. (2024). Their scheme included two new reactions: production of hydrogen chloride via heterogeneous reaction of atomic hydrogen with mineral dust, and the heterogeneous adsorption of HCl onto water ice surfaces, both adapted from Krasnopolsky (2022).

In the case that chlorine salts are the origin of gas-phase HCl in the atmosphere of Mars, a major issue that results from the above mechanisms is that the surface reservoir of chlorine is being cycled on a seasonal scale from one type into another. As we will discuss below, there is currently no proposed mechanisms for HCl removal that will return it to a chloride salt, such as NaCl. In the case that HCl is converted into perchlorate and deposited on the surface Catling et al. (2010), M. L. Smith et al. (2014), we would be observing an annual resurfacing of surface perchlorate and the gradual depletion of chloride salts on the surface. This rapid resurfacing is still an issue for the case of HCl being sourced from perchlorate and cycled back into perchlorate deposits. Current orbital observations of widespread surface chlorides favor simple metal salts (Glotch et al., 2016), while also indicating that perchlorates may be widespread (Clark & Kounaves, 2016). Studies of surface chloride deposits also indicate that they occurred on the order of billions of years, rather than being a contemporary activity (Leask & Ehlmann, 2022; Martin et al., 2020).

3.2. Sourced From the Surface

HCl was a target gas for the ExoMars TGO mission due its close terrestrial links with active volcanism. Its discovery in the Martian atmosphere may be the first direct evidence of active volcanic or subsurface magmatic activity. However, we would also expect to have found other volcanic gases in the Martian atmosphere if this were the case. So far TGO instruments have only reported very low upper limits of sulfur-bearing compounds (Braude et al., 2022) and organic gases, including methane (Knutsen et al., 2021; Korablev et al., 2019; Montmessin et al., 2021). The observed, repeated seasonal cycles (see part 1; Olsen et al., 2024b) are also difficult to reconcile with a surface source.

In order for a surface emission to source gas-phase chloride seasonally, the source must be affected by seasonal activity on the surface, which is mostly related to frosts and the annual freeze-thaw cycles of H_2O and CO_2. Low-level magmatic activity at high latitudes may not be able to release trace gases due to an overburden of ice and frost. Likewise for pockets of trapped gas from ancient volcanic activity. Either process would also require the subsurface alterations to produce a proportion of chlorides to sulphides that is slightly greater than on Earth. Volcanic emission contain 5–10 times the amount of SO_2 than HCl (e.g., Stremme et al., 2023, and references therein), while our upper limits for SO_2 are between 10 and 50 ppbv (abundance expected alongside 3–5 ppbv HCl is 15–75 ppbv SO_2).

There is also the possibility that there are subsurface HCl stores held below the southern polar ice cap that begin to seep trace gases as the frost sublimates each year. Gas may be stored within the polar ice as well, in inclusions in the ice or as part of a clathrate. Chlorine hydrates are the earliest identified clathrate (Davy, 1811), but are not known to occur naturally on Earth. The stability of methane clathrates has been modeled for Martian conditions (Stevens et al., 2015, 2017), which gives an indication of the likely stability of chlorine hydrates. The depth at which methane clathrates are stable was shown to be reduced by the presences of chloride salts (Gloesener et al., 2021). Since the annual extent of polar ice cap formation and recession is stable on contemporary Mars, it is unlikely that these types of HCl storage are a viable solution to our observations since they have no way of being replenished and would most likely be depleted since the previous periods of major volcanic activity.

Rather than ancient chlorides trapped within polar ice stores, HCl may be adhered to the seasonally replenished ice pack. In Section 3.5 we will introduce loss processes by which gas-phase HCl adheres to aerosol particles and is deposited back to the surface. This process would lead to a seasonally replenishing, ice-bound chloride reservoir. Each spring, sublimation of water vapor frosts would lead to a growth in the HCl VMR. This type of

source forms a closed-loop in the chlorine chemistry by not requiring the transformation between distinct chloride reservoirs, as a photochemical dust source implies.

3.3. Photochemical Loss

A possible loss pathways for HCl is the formation of ClO, which can eventually lead to the formation of perchlorate (ClO_4^-) being deposited on the surface. This has been promoted as an explanation for perchlorate measurements on the Martian surface (Glavin et al., 2013; Hecht et al., 2009) based on its terrestrial occurrences in the Atacama desert (Catling et al., 2010). This hypothesis used volcanic HCl as a source, and modeled perchlorate formation over geological time scales, rather than seasonally, and from a larger, replenishing source amount of HCl. More recent modeling studies have shown that ClO and ClO_4^- bonds do occur over the observed seasonal time scales (Rajendran et al., 2024) but not that HCl can be rapidly removed and suddenly undergo complete destruction.

The method by which Catling et al. (2010) describes the perchlorate formation process begins with the formation of OClO. Isomers of ClO_2 can be formed via a self-reaction of ClO, but are also formed by ClO on ice as it sublimates. The final stage in the reaction chain is between ClO_3 and OH. At the end of southern summer, when we observe a rapid decline of HCl, these processes become unfavorable, due to the continuing cooling of the Martian atmosphere and reduction of water vapor and OH. As with Cl sourced from dust, this process is generally one-way, converting HCl into ClO_4^- without providing a suitable mechanism for replenishing HCl.

3.4. Dynamic Loss

An important aspect of the water cycle on Mars is the seasonal increase in the hygropause height (e.g., Aoki et al., 2022; Fedorova et al., 2023; Heavens et al., 2018; Montmessin et al., 2017). While this is caused by the atmosphere warming and the south polar hood sublimating, it is a reflection of the thermal expansion of the lower atmosphere (Neary et al., 2020), rather than an injection of water vapor. At the end of southern summer, the south polar hood is reforming and the hygropause is again lowered. High VMRs of water vapor (>150–200 ppmv; e.g., Figure S4 in Supporting Information S1) are observed during northern summer, but they are restricted to altitudes below 5–10 km.

Two processes occur to control the hygropause height: reduction in both atmospheric temperature and pressure cause the atmosphere to contract, bringing trace gases such as water vapor and HCl closer to the surface; and the cooling atmosphere causes the condensation of water vapor at the hygropause height and above. HCl is not condensible, but the rapid reduction of OH and HO_2 needed to produce HCl will severely limit its production rate. HCl and H_2O are very closely correlated, as shown in part 1 and Figure 6, and the reduction in the vertical extent of HCl occurs at the southern summer solstice and continues until the end of southern summer, which tracks that of water vapor (Olsen et al., 2024b). The possibility remains, therefore, that HCl is limited to the near-surface atmosphere, where ACS solar occultations have difficulty making observations, coupled with a reduction in its source strength.

3.5. Heterogeneous Loss

A major removal process for atmospheric chlorine in Earth's troposphere, especially when sourced from sea salt aerosols, is wet and dry deposition. Terrestrially, only a small percentages (<5%) of chloride sourced from sea salt aerosols remains in the atmosphere in a gas phase. The remainder will re-attach itself to mineral aerosols or water surfaces (liquid and ice) and fall back to the surface (e.g., X. Wang et al., 2019). In the absence of water outside the vapor form on Mars at the altitudes and time periods where HCl is observed, HCl would instead have to bond to dust aerosols, which is an effective process in Earth's atmosphere (Ooki & Uematsu, 2005; Sullivan et al., 2007; Tobo et al., 2010).

To explain our observations of Martian HCl, we would consider such a process to be dependant on the abundance of dust and to be occurring throughout the perihelion period. At the same time, HCl on the surface of dust aerosols would be released back into the atmosphere at a rate which would allow an equilibrium to be reached. At the end of southern summer, as the dust top lowers toward the surface, so does HCl. When dust activity terminates, it may take with it the majority of the atmospheric chloride reservoir.

Similarly, HCl will efficiently bond to condensed water ice aerosols (Crowley et al., 2010; Kippenberger et al., 2019). Unlike with dust, this will not be an ongoing process. As we showed in part 1, HCl occurs at altitudes only where the atmosphere is sufficiently warm enough to host water vapor, with ice occurring above our HCl observations and outlining the hygropause (Olsen et al., 2024b). While we expect water vapor and HO_2 to define the altitude range over which HCl is produced, we also expect HCl to stably remain in the atmosphere when water vapor condenses, since HCl will not. We consistently do not observe HCl at altitudes higher than water vapor. Around the southern summer solstice, HCl and dust coexist at altitudes up to 30–40 km, but ice is only present above the dust layer and hygropause. Therefore, this process becomes increasingly important toward the autumnal equinox as the hygropause lowers and the altitudes at which water ice forms are reduced.

HCl adhering to water ice aerosol surfaces may be an effective sink that can explain our observations. In the final period of southern summer, after the late-season storm, we observe a rapid cooling throughout the lower atmosphere which is accompanied by a rapid reduction in the VMRs of both water vapor and HCl. At this time, water ice is forming throughout an altitude range from 50 km down to ∼15 km (see part 1; Olsen et al., 2024b). If HCl production path is removed by the reduction of water vapor, and there are enough ice surfaces, and the heterogeneous process is rapid enough, then the reduction of the HCl VMR to below our detection threshold may be explained by the replacement of water vapor by ice. Luginin et al. (2024) found an evidence of such rapid HCl uptake on water ice using simultaneous measurements from ACS MIR and aerosol abundances from the ACS thermal-infrared channel (TIRVIM). This is also supported by modeling (Taysum et al., 2024).

At altitudes above 30 km, this process may be occurring throughout southern summer and controlling the height of HCl throughout the season. From the early major dust storms through to the late season storms, we observe a steady decline in hygropause height. This is matched by HCl, a water ice layer, and a temperature isotherm (see part 1; Olsen et al., 2024b). Condensing water vapor may be scavenging the remaining HCl from the gas phase at these heights.

The most important aspect of this loss process is the fate of HCl, which is now sequestered on ice surface in the air and, later, the surface. When temperatures warm again and ice sublimates it will release both water vapor and HCl. Unlike several mechanisms discussed, this provides a closed loop for the atmospheric chloride cycle, without requiring conversion between reservoirs—the HCl source and sink are seasonally varying surface frosts.

Aphelion observations prove a challenge to this hypothesis, however (further discussed in Section 3.7). HCl is distributed across both hemispheres, appearing and disappearing simultaneously at the beginning of southern spring and end of southern summer. HCl removal by ice and subsequent surface deposition should occur to some extent at high northern latitudes. However, during northern summer, when surface ice near the northern polar ice cap has sublimated and there are significant amounts of water vapor in the lower atmosphere, HCl is generally not present. If the source is entirely in the south and HCl observed in the north is due to Hadley cell transport north from the southern sub-solar point, it would not be bound by the hygropause.

This mechanism also has implications for observations of surface chloride deposits that occur across the Martian surface (Glotch et al., 2010; Murchie et al., 2009; Osterloo et al., 2008, 2010; Ruesch et al., 2012; Wray et al., 2009). In these cases, the specific chloride molecule cannot be identified, but if HCl is trapped on ice surface, it becomes a candidate. In this case, these may be a correlation between chloride observations and frosts, and the chloride deposits will not be permanently located.

3.6. Atmospheric Cl as a Reservoir

Rather than a specific HCl destruction process, one possibility to explain our results is that chlorine resides in the atmosphere as a gas throughout the year, but in a different form than HCl. This was not initially considered a possibility as HCl was expected to be the longest living stable chlorine reservoir (with greater abundances than $ClONO_2$) and requires faster rates of photolysis than expected (Krasnopolsky et al., 1997; Lefèvre & Krasnopolsky, 2017). Photochemical modeling studies are ongoing to determine whether this is a viable option.

HCl is expected to rapidly photolyze into H and Cl (rate coefficient similar to ozone), but the atomic hydrogen will contribute to the re-formation of HO_2 which will most likely lead to the reformation of HCl. A reduction of HCl would have to come from the formation of a bond between Cl and oxygen, and this process would otherwise be neutral. As southern fall approaches and the atmosphere cools and contracts, the VMR of water vapor drops off rapidly as it condenses. This will take with it OH and HO_2. What may be happening over the equinox and into the

aphelion period is that HCl is undergoing rapid photolysis, but the reduction in OH and HO_2 prevent the reformation of HCl.

In this case, reactive Cl would be mainly forming ClO (Cl does not self-react to form Cl_2; for a review of Cl reactions see Catling et al., 2010; Krasnopolsky, 2022). ClO is less stable than HCl and will also photolyze, allowing Cl to cycling between the atomic radical and its oxidants. Due to the reduction of HCl and water vapor photolysis products at this time, the most likely formation mechanism is via reaction with ozone, which is building over the equinox (see Section 2.5). While the ClO photolysis rate is similar to that of HCl, the reaction $ClO + O - Cl + O_2$ is several time faster than that between ClO and O_3 (Catling et al., 2010; Krasnopolsky, 2022).

These reactions may allow Cl to remain in the gas phase without forming detectable levels of HCl over the aphelion period. Dedicated modeling work is needed to show this, and Rajendran et al. (2024) and Streeter et al. (2024) have already shown that a build up of Cl will occur over the aphelion period. The northern spring conditions modeled by Krasnopolsky (2022) resulted HCl abundances below the ACS detection limits, but also a very low abundance of Cl. This process would also be coupled to those discussed previously: the contraction of the atmosphere may limit Cl residence to below 5–10 km, diminishing the solar occultation technique's opportunities for detection, and the formation of heavier chlorine oxides or the adherence to dust and ice aerosol particles may lead to deposition.

3.7. Aphelion HCl

In MY 35 we made two definitive detections of HCl after the end of southern summer. These were made at high northern latitudes at $L_s = 109°$ and 115° over the Alba Fossae and the Tantalus Fossae (Olsen, Trokhimovskiy, et al., 2021). In MY 36, a single definitive detection of HCl was made over the aphelion period, this time at $L_s = 105°$, but over the same geographical region. We initiated a dedicated search for HCl over the Arcadia region in MY 37 (results forthcoming) in order to investigate further.

The geographic area over which these observations are made is a relatively high elevation plateau in the high northern latitudes. This reduces the atmospheric density and dust loading making for ideal observation conditions for detecting trace gases with ACS MIR. The time frame, just after the northern summer solstice, is coincident with the period of peak dust activity at northern latitudes for MYs 34–36 (Montabone et al., 2020). Specifically, a regional dust storm over this area was observed in MY 36 by the Emirates Mars Mission (Gebhardt et al., 2022).

The first thing to note about these observations is that they are not inconsistent with those made during southern spring and summer. HCl is restricted to the lower atmosphere, below 5–10 km, and demonstrates a correlation with water vapor, itself restricted to those low altitude levels (Olsen, Trokhimovskiy, et al., 2021). HCl occurs coincidental with dust loading, and only in regions of the atmosphere where it is warm enough to prevent water ice formation (ice forms above 20 km in the northern hemisphere during northern spring and summer). The observations are made at northern latitudes (45°–65°N) where seasonal frosts should accumulate. The previously discussed mechanisms for HCl formation and destruction are not excluded at this time.

A second thing to note is that the atmospheric conditions for these HCl observations are not unique. In the solar occultation mode, we are not making frequently repeated observations over specific areas, especially with the changing secondary grating position required for HCl detection. Figure S4 in Supporting Information S1 shows the MY 35 vertical profiles of HCl (Olsen, Trokhimovskiy, et al., 2021), as well as several other simultaneous ACS NIR and co-located MCS observations between $L_s = 105°$ and 120° (while these are restricted to northern latitudes, all longitudes are allowed). The HCl occurs at low altitudes that are generally probed by ACS. One of the observations occurred within the nominal range of temperatures and water vapor VMRs, while the other occurred during a warmer and wetter condition. Both occurred with elevated, but average, dust opacities, but very low water ice opacities. However, this period also coincides with an O_3 column abundance minimum observed by the ultraviolet channel of NOMAD (Mason et al., 2024).

Throughout the aphelion period, we are making low-altitude measurements of water vapor abundance in the presence of dust, but without an absorption signal for HCl. This is an aspect more inconsistent with the mechanisms proposed than the detection of HCl. If dust were a source, we would expect more frequent detections over a wider area. If dust were a source, but an energetic phenomenon such as electrostatic discharges (A. Wang et al., 2020; A. Wang et al., 2023) were required, then there is a possibility that this time period may be favored

due it having the maximum aphelion dust opacities. If dust breakdown under UV was the source, this period would be disadvantaged by reduced UV flux at aphelion. If water ice formation were a loss mechanism, we would also expect the observed abundances of HCl at northern latitudes to remain in that hemisphere, form frosts over the equinox, and sublimate again in northern summer. This is consistent with the aphelion observations, but also suggests that HCl should be found over a wider area and time period.

A key seasonal difference in the atmospheric conditions of the perihelion and aphelion HCl observations is the amount of odd-oxygen. The atmosphere is sufficiently cold enough and depleted of OH and HO_2 to allow the build up of ozone at all latitudes (greater in the south than the north). The Martian northern hemisphere tends to have peak O_3 abundances between 20 and 30 km, but being depleted toward the surface where water vapor is present (Olsen et al., 2022). As discussed in Section 2.5, odd-oxygen may regulate HCl abundance, reducing its VMR over aphelion, even if it were being produced at the same time. This may also lead to a more efficient ClO-dominant atmosphere since atomic oxygen and HCl lead to ClO, while O_3 and Cl reactions also form ClO.

4. Conclusion

In part 1 of this two-part study we presented three Mars years of the climatologies of HCl and H_2O as their change in VMR vertical profiles over solar longitude (Olsen et al., 2024b). We compared the climatological cycles of the gas VMRs to those of the temperatures from ACS NIR and the opacities of dust and water ice aerosols from MCS. This comparison showed that HCl abundances tracked those of water vapor very closely in season and vertical extent. We also showed that dust lifting played a strong role in driving the atmospheric temperatures, which in turn controlled the hygropause height and water ice distribution. This confirmed temporal correlations between HCl and both dust and ice aerosols.

Here, in part 2, we quantified the correlations between these quantities and revealed a strong positive correlation between water vapor and HCl. This confirms their expected photochemical dependence in which H_2O photolysis products are necessary to form HCl from Cl. A moderate correlation was found between water vapor and dust which confirms the impact that dust has on the water vapor content of the Martian atmosphere. A moderate anti-correlation with ice was also found which indicates that the formation of water ice comes at the expense of vapor.

All three quantities are also strongly correlated to temperature. In the case of dust opacity, a positive correlation indicates the greenhouse effect created by airborne dust intercepting solar radiation. This leads to a strong correlation between temperatures and water vapor. The strong anti-correlation between temperature and ice opacity highlights the control that changing temperatures have on ice formation and sublimation.

Despite the strong correlation between water vapor and HCl, and the relationships between H_2O and the other studied parameters, we found only weak correlations between HCl and either aerosol, and only a moderate correlation between HCl and temperature. This result does not support a direct link between airborne dust and HCl formation. Because dust is always present coincidentally with HCl (unlike ice), it also cannot explain the sudden reduction in HCl at the end of southern.

Each formation and destruction process that we discussed is possible and supported by either terrestrial observations or laboratory studies. That chloride-bearing dust can release Cl ions for reaction and the production of HCl is certain, but its efficiency and relative importance remain to be determined. Another issue with such a source mechanism is that it is irreversible, and therefore unsustainable given the seasonality of HCl (similarly for rapid photochemical loss). The rate at which chloride salts, such as NaCl, are being destroyed, while oxychlorides, such as perchlorate, are being produced is unlikely to be able to produce the observed seasonal cycle of HCl.

Likewise, another unfavorable solution is that chloride remains in the lower atmosphere throughout the Martian year. While a cycle between Cl and ClO is possible, the amount of water vapor present at northern latitudes, and the infrequency of aphelion observations make this unlikely. Ozone will certainly play a role in the regulation of HCl abundances, but is also unlikely to be solely responsible for its seasonal loss.

Despite the low anti-correlation with water ice, the adherence to ice aerosols remains the most likely loss mechanism to explain our results. Its plausibility is strengthened by forming a closed loop by also becoming a plausible source mechanism after surface deposition of HCl-loaded water ice aerosols. In this case, HCl remains the long-lived stable chlorine reservoir. That there may be a connection between ices and HCl despite their low anti-correlation comes from their distinct residence heights. HCl, strongly correlated with water vapor, resides at

altitudes below the hygropause and the water ice layers—it is when those move toward the surface that HCl becomes undetectable.

In this work, we have characterized HCl, both in terms of its behavior and interactions. HCl is currently the only novel trace gas detected in the Martian atmosphere over the ExoMars TGO mission, and its characterization and the determination of its sources and sinks remains a top objective of the ExoMars mission. We have identified several possible mechanisms for production or removal of HCl, some of which are currently being investigated with the use of photochemical models. The correlation magnitudes between HCl and water vapor, temperature, water ice opacity, and dust opacity have provided important information about the likelihood that each HCl source and sink are responsible for our observations. We have shown that interactions with dust and oxidation play roles in HCl behavior, but may not be individually responsible for its seasonal cycle. Work remains to determine the relative importance and rates of each mechanism. Especially needed are measurements of and modeling of the rate of HCl take up on ice surfaces, the efficiency of interactions between HCl and ozone, and the localization of HCl in northern summer.

Conflict of Interest

The authors declare no conflicts of interest relevant to this study.

Data Availability Statement

The VMR vertical profiles generated in this study are available on the Oxford Research Archive (Olsen et al., 2024a). The data sets generated by the ExoMars Trace Gas Orbiter instruments analyzed in this study are made available in the European Space Agency (ESA) Planetary Science Archive (PSA) repository (European Space Agency, 2023), following a 6 months prior access period, and the ESA Rules on Information, Data and Intellectual Property. Temperature and pressure data used here are from ACS NIR and were generated in other studies: data from MY 34 are made available in Fedorova et al. (2020) and an updated data version containing MYs 34–36 are published in Fedorova et al. (2023). Data from the MCS investigation (v5.2) are made available through the NASA Planetary Data System (PDS; NASA, 2017). The LMD MCD v5.3 and v6.1 as well as data generated with the PCM for TGO solar occultations, along with its user guide, are hosted by LMD (LMD, 2018).

Acknowledgments
This work was funded by the UK Space Agency (ST/T002069/1, ST/Y000196/1). The ExoMars mission is a joint mission of the European Space Agency (ESA) and Roscosmos. The ACS investigation was developed by the Laboratoire Atmosphères, Milieux, Observations Spatiales (LATMOS/CNRS) in Paris and the Space Research Institute (IKI) in Moscow. The investigation was funded by the National Centre for Space Studies of France (CNES) and Roscosmos. The GGG software suite is maintained at JPL (tccon-wiki.caltech.edu). A.F., A.T., O.K. and D.B. acknowledge funding from RSF (Russian Science Foundation; 23-12-00207). LATMOS affiliates acknowledge funding from CNES and ANR (PRCI, CE31 AAPG2019-MCUBE project). Open University affiliates acknowledge funding from the UK Space Agency (ST/V002295/1, ST/W00268X/1, ST/W002949/1, ST/V002295/1, ST/V005332/1, ST/X006549/1 and ST/Y000234/1). Work at the Jet Propulsion Laboratory, California Institute of Technology, was performed under contract with the National Aeronautics and Space Administration (80NM0018D0004). MCS data and assistance were provided by D.M.K. and A.K. and additional processing was performed by P.S. and J.A.H. All spectral fitting of ACS MIR data was performed by K.S.O. using the GGG software suite. Temperature and pressure data from ACS NIR were provided by A.A.F. Processing of ACS spectra is done by A.T. at IKI and by L.B. at LATMOS by L.B. Input and aid on spectral fitting, and on interpretation of data, were given by J.A., D.A.B., A.A.F., F.M., F.L., M.R.P., and J.M. Atmospheric modeling and insight into atmospheric chemistry was performed by K.R. and P.S. The ACS instrument was designed, developed, and operated by A.P., A.S., A.T., F.M., and O.K. We would like to thank Duhita Naware and Mhairi Reid for consulting on color schemes for Figure 1, and to Glenn Orton for kindly reviewing our manuscript prior to submission.

References

Aoki, S., Daerden, F., Viscardy, S., Thomas, I. R., Erwin, J. T., Robert, S., et al. (2021). Annual appearance of hydrogen chloride on Mars and a striking similarity with the water vapor vertical distribution observed by TGO/NOMAD. *Geophysical Research Letters*, *48*(11). https://doi.org/10.1029/2021gl092506

Aoki, S., Vandaele, A. C., Daerden, F., Villanueva, G. L., Liuzzi, G., Clancy, R. T., et al. (2022). Global vertical distribution of water vapor on Mars: Results from 3.5 years of ExoMars-TGO/NOMAD science operations. *Journal of Geophysical Research*, *127*(9). https://doi.org/10.1029/2022je007231

Atreya, S. K., Wong, A.-S., Renno, N. O., Farrell, W. M., Delory, G. T., Sentman, D. D., et al. (2006). Oxidant enhancement in Martian dust devils and storms: Implications for life and habitability. *Astrobiology*, *6*(3), 439–450. https://doi.org/10.1089/ast.2006.6.439

Braude, A. S., Montmessin, F., Olsen, K. S., Trokhimovskiy, A., Korablev, O. I., Lefèvre, F., et al. (2022). No detection of SO2, H2S, or OCS in the atmosphere of Mars from the first two Martian years of observations from TGO/ACS. *Astronomy & Astrophysics*, *658*, A86. https://doi.org/10.1051/0004-6361/202142390

Bridges, J. C., & Grady, M. M. (1999). A halite-siderite-anhydrite-chlorapatite assemblage in Nakhla: Mineralogical evidence for evaporites on Mars. *Meteoritics & Planetary Science*, *34*(3), 407–415. https://doi.org/10.1111/j.1945-5100.1999.tb01349.x

Bridges, J. C., & Grady, M. M. (2000). Evaporite mineral assemblages in the nakhlite (Martian) meteorites. *Earth and Planetary Science Letters*, *176*(3), 267–279. https://doi.org/10.1016/S0012-821X(00)00019-4

Brown, M. A. J., Patel, M. R., Lewis, S. R., Holmes, J. A., Sellers, G. J., Streeter, P. M., et al. (2022). Impacts of heterogeneous chemistry on vertical profiles of Martian ozone. *Journal of Geophysical Research*, *127*(11). https://doi.org/10.1029/2022je007346

Carrier, B. L., & Kounaves, S. P. (2015). The origins of perchlorate in the Martian soil. *Geophysical Research Letters*, *42*(10), 3739–3745. https://doi.org/10.1002/2015GL064290

Catling, D. C., Claire, M. W., Zahnle, K. J., Quinn, R. C., Clark, B. C., Hecht, M. H., & Kounaves, S. (2010). Atmospheric origins of perchlorate on Mars and in the Atacama. *Journal of Geophysical Research*, *115*(E1). https://doi.org/10.1029/2009je003425

Clancy, R. T., Wolff, M. J., Lefèvre, F., Cantor, B. A., Malin, M. C., & Smith, M. D. (2016). Daily global mapping of Mars ozone column abundances with MARCI UV band imaging. *Icarus*, *266*, 112–133. https://doi.org/10.1016/j.icarus.2015.11.016

Clark, B. C., & Kounaves, S. P. (2016). Evidence for the distribution of perchlorates on Mars. *International Journal of Astrobiology*, *15*(4), 311–318. https://doi.org/10.1017/S1473550415000385

Crowley, J. N., Ammann, M., Cox, R. A., Hynes, R. G., Jenkin, M. E., Mellouki, A., et al. (2010). Evaluated kinetic and photochemical data for atmospheric chemistry: Volume V – Heterogeneous reactions on solid substrates. *Atmospheric Chemistry and Physics*, *10*(18), 9059–9223. https://doi.org/10.5194/acp-10-9059-2010

Davy, H. (1811). On a combination of oxymuriatic gas and oxygene gas. *Philosophical Transactions of the Royal Society of London*, 101. https://doi.org/10.1098/rstl.1811.0008

European Space Agency. (2023). ExoMars 2016 ACS calibrated data product collection (V104.1) [Dataset]. *European Space Agency*. https://doi.org/10.57780/ESA-RTLH14G

Fedorova, A. A., Montmessin, F., Korablev, O., Luginin, M., Trokhimovskiy, A., Belyaev, D. A., et al. (2020). Stormy water on Mars: The distribution and saturation of atmospheric water during the dusty season. *Science*, *367*(6475), 297–300. https://doi.org/10.1126/science.aay9522

Fedorova, A. A., Montmessin, F., Trokhimovskiy, A., Luginin, M., Korablev, O., Alday, J., et al. (2023). A two-Martian year survey of the water vapor saturation state on Mars based on ACS NIR/TGO occultations. *Journal of Geophysical Research*, *128*(1), e2022JE007348. https://doi.org/10.1029/2022JE007348

Gebhardt, C., Guha, B. K., Young, R. M. B., & Wolff, M. J. (2022). A frontal dust storm in the northern hemisphere at solar longitude 97—An unusual observation by the Emirates Mars mission. *Geophysical Research Letters*, *49*(20). https://doi.org/10.1029/2022gl099528

George, I. J., & Abbatt, J. P. D. (2010). Heterogeneous oxidation of atmospheric aerosol particles by gas-phase radicals. *Nature Chemistry*, *2*(9), 713–722. https://doi.org/10.1038/nchem.806

Giuranna, M., Wolkenberg, P., Grassi, D., Aronica, A., Aoki, S., Scaccabarozzi, D., et al. (2021). The current weather and climate of Mars: 12 years of atmospheric monitoring by the planetary fourier spectrometer on Mars express. *Icarus*, *353*, 113406. https://doi.org/10.1016/j.icarus.2019.113406

Glavin, D. P., Freissinet, C., Miller, K. E., Eigenbrode, J. L., Brunner, A. E., Buch, A., et al. (2013). Evidence for perchlorates and the origin of chlorinated hydrocarbons detected by SAM at the Rocknest Aeolian deposit in Gale Crater. *Journal of Geophysical Research*, *118*(10), 1955–1973. https://doi.org/10.1002/jgre.20144

Gloesener, E., Karatekin, O., & Dehant, V. (2021). Stability and composition of CH_4-rich clathrate hydrates in the present Martian subsurface. *Icarus*, *353*, 114099. https://doi.org/10.1016/j.icarus.2020.114099

Glotch, T. D., Bandfield, J. L., Tornabene, L. L., Jensen, H. B., & Seelos, F. P. (2010). Distribution and formation of chlorides and phyllosilicates in Terra Sirenum, Mars. *Geophysical Research Letters*, *37*(16). https://doi.org/10.1029/2010GL044557

Glotch, T. D., Bandfield, J. L., Wolff, M. J., Arnold, J. A., & Che, C. (2016). Constraints on the composition and particle size of chloride salt-bearing deposits on Mars. *Journal of Geophysical Research*, *121*(3), 454–471. https://doi.org/10.1002/2015JE004921

Goetz, W., Bertelsen, P., Binau, C. S., Gunnlaugsson, H. P., Hviid, S. F., Kinch, K. M., et al. (2005). Indication of drier periods on Mars from the chemistry and mineralogy of atmospheric dust. *Nature*, *436*(7047), 62–65. https://doi.org/10.1038/nature03807

Graedel, T. E., & Keene, W. C. (1995). Tropospheric budget of reactive chlorine. *Global Biogeochemical Cycles*, *9*(1), 47–77. https://doi.org/10.1029/94GB03103

Graedel, T. E., & Keene, W. C. (1996). The budget and cycle of Earth's natural chlorine. *Pure and Applied Chemistry*, *68*(9), 1689–1697. https://doi.org/10.1351/pac199668091689

Haider, S., Siddhi, Y., Masoom, J., Sheel, V., & Kuroda, T. (2022). Impact of dust loading on ozone, winds and heating rates in the atmosphere of Mars: Seasonal variability, climatology and SPICAM observations. *Planetary and Space Science*, *212*, 105424. https://doi.org/10.1016/j.pss.2022.105424

Heavens, N. G., Kleinböhl, A., Chaffin, M. S., Halekas, J. S., Kass, D. M., Hayne, P. O., et al. (2018). Hydrogen escape from Mars enhanced by deep convection in dust storms. *Nature Astronomy*, *2*(2), 126–132. https://doi.org/10.1038/s41550-017-0353-4

Hecht, M. H., Kounaves, S. P., Quinn, R. C., West, S. J., Young, S. M. M., Ming, D. W., et al. (2009). Detection of perchlorate and the soluble chemistry of Martian soil at the Phoenix lander site. *Science*, *325*(5936), 64–67. https://doi.org/10.1126/science.1172466

Holmes, J. A., Lewis, S. R., Patel, M. R., & Lefèvre, F. (2018). A reanalysis of ozone on Mars from assimilation of SPICAM observations. *Icarus*, *302*, 308–318. https://doi.org/10.1016/j.icarus.2017.11.026

Keene, W. C., Khalil, M. A. K., Erickson, D. J., McCulloch, A., Graedel, T. E., Lobert, J. M., et al. (1999). Composite global emissions of reactive chlorine from anthropogenic and natural sources: Reactive Chlorine Emissions Inventory. *Journal of Geophysical Research*, *104*(D7), 8429–8440. https://doi.org/10.1029/1998jd100084

Kippenberger, M., Schuster, G., Lelieveld, J., & Crowley, J. N. (2019). Trapping of HCl and oxidised organic trace gases in growing ice at temperatures relevant to cirrus clouds. *Atmospheric Chemistry and Physics*, *19*(18), 11939–11951. https://doi.org/10.5194/acp-19-11939-2019

Kleinböhl, A., Friedson, A. J., & Schofield, J. T. (2017). Two-dimensional radiative transfer for the retrieval of limb emission measurements in the Martian atmosphere. *Journal of Quantitative Spectroscopy and Radiative Transfer*, *187*, 511–522. https://doi.org/10.1016/j.jqsrt.2016.07.009

Kleinböhl, A., Schofield, J. T., Kass, D. M., Abdou, W. A., Backus, C. R., Sen, B., et al. (2009). Mars Climate Sounder limb profile retrieval of atmospheric temperature, pressure, and dust and water ice opacity. *Journal of Geophysical Research*, *114*(E13), E10006. https://doi.org/10.1029/2009JE003358

Kleinböhl, A., Spiga, A., Kass, D. M., Shirley, J. H., Millour, E., Montabone, L., & Forget, F. (2020). Diurnal variations of dust during the 2018 global dust storm observed by the Mars climate sounder. *Journal of Geophysical Research*, *125*(1), e2019JE006115. https://doi.org/10.1029/2019je006115

Knipping, E. M., & Dabdub, D. (2002). Modeling Cl2 formation from aqueous NaCl particles: Evidence for interfacial reactions and importance of Cl_2 decomposition in alkaline solution. *Journal of Geophysical Research*, *107*(D18), ACH 8-1. https://doi.org/10.1029/2001JD000867

Knutsen, E. W., Villanueva, G. L., Liuzzi, G., Crismani, M. M. J., Mumma, M. J., Smith, M. D., et al. (2021). Comprehensive investigation of Mars methane and organics with ExoMars/NOMAD. *Icarus*, *357*, 114266. https://doi.org/10.1016/j.icarus.2020.114266

Korablev, O., Olsen, K. S., Trokhimovskiy, A., Lefèvre, F., Montmessin, F., Fedorova, A. A., et al. (2021). Transient HCl in the atmosphere of Mars. *Science Advances*, *7*(7), eabe4386. https://doi.org/10.1126/sciadv.abe4386

Korablev, O., Vandaele, A. C., Montmessin, F., Fedorova, A. A., Trokhimovskiy, A., Forget, F., et al. (2019). No detection of methane on Mars from early ExoMars trace gas orbiter observations. *Nature*, *568*(7753), 517–520. https://doi.org/10.1038/s41586-019-1096-4

Krasnopolsky, V. A. (2022). Photochemistry of HCl in the Martian atmosphere. *Icarus*, *374*, 114807. https://doi.org/10.1016/j.icarus.2021.114807

Krasnopolsky, V. A., Bjoraker, G. L., Mumma, M. J., & Jennings, D. E. (1997). High-resolution spectroscopy of Mars at 3.7 and 8 μm: A sensitive search for H_2O_2, H_2CO, HCl, and CH_4, and detection of HDO. *Journal of Geophysical Research*, *102*(E3), 6525–6534. https://doi.org/10.1029/96JE03766

Ladino, L. A., & Abbatt, J. P. D. (2013). Laboratory investigation of Martian water ice cloud formation using dust aerosol simulants. *Journal of Geophysical Research*, *118*(1), 14–25. https://doi.org/10.1029/2012JE004238

Laskin, A., Wang, H., Robertson, W. H., Cowin, J. P., Ezell, M. J., & Finlayson-Pitts, B. J. (2006). A new approach to determining gas-particle reaction probabilities and application to the heterogeneous reaction of deliquesced sodium chloride particles with gas-phase hydroxyl radicals. *Journal of Physical Chemistry A*, *110*(36), 10619–10627. https://doi.org/10.1021/jp063263

Leask, E. K., & Ehlmann, B. L. (2022). Evidence for deposition of chloride on Mars from small-volume surface water events into the late Hesperian-early Amazonian. *AGU Advances*, *3*(1). https://doi.org/10.1029/2021av000534

Lebonnois, S., Quémerais, E., Montmessin, F., Lefèvre, F., Perrier, S., Bertaux, J.-L., & Forget, F. (2006). Vertical distribution of ozone on Mars as measured by SPICAM/Mars express using stellar occultation's. *Journal of Geophysical Research*, *111*(E9), E09S05. https://doi.org/10.1029/2005JE002643

Lefèvre, F., & Krasnopolsky, V. (2017). Atmospheric photochemistry. In R. M. Haberle, R. T. Clancy, F. Forget, M. D. Smith, & R. W. Zurek (Eds.), *The atmosphere and climate of Mars* (pp. 405–432). Cambridge University Press.

Lefèvre, F., Trokhimovskiy, A., Fedorova, A., Baggio, L., Lacombe, G., Määttänen, A., et al. (2021). Relationship between the ozone and water vapor columns on Mars as observed by SPICAM and calculated by a Global Climate Model. *Journal of Geophysical Research*, *126*(4), e2021JE006838. https://doi.org/10.1029/2021JE006838

LMD. (2018). The Mars climate database projects (v6.1) [Dataset]. *LMD*. https://www-mars.lmd.jussieu.fr/

Luginin, M., Trokhimovskiy, A., Taysum, B., Fedorova, A. A., Korablev, O., Olsen, K. S., et al. (2024). Evidence of rapid hydrogen chloride uptake on water ice in the atmosphere of Mars. *Icarus*, *411*, 115960. https://doi.org/10.1016/j.icarus.2024.115960

Madeleine, J.-B., Forget, F., Millour, E., Montabone, L., & Wolff, M. J. (2011). Revisiting the radiative impact of dust on Mars using the LMD global climate model. *Journal of Geophysical Research*, *116*(E15), E11010. https://doi.org/10.1029/2011je003855

Maguire, W. C. (1977). Martian isotopic ratios and upper limits for possible minor constituents as derived from Mariner 9 infrared spectrometer data. *Icarus*, *32*(1), 85–97. https://doi.org/10.1016/0019-1035(77)90051-3

Martin, P. E., Farley, K. A., Douglas, A. P., Hogancamp, J. V., Siebach, K. L., Grotzinger, J. P., & McLennan, S. M. (2020). Reevaluation of perchlorate in Gale Crater Rocks suggests geologically recent perchlorate addition. *Journal of Geophysical Research*, *125*(2). https://doi.org/10.1029/2019je006156

Martz'inez-Pabello, P. U., Navarro-González, R., Walls, X., Pi-Puig, T., González-Chávez, J. L., de la Rosa, J. G., et al. (2019). Production of nitrates and perchlorates by laser ablation of sodium chloride in simulated Martian atmospheres. Implications for their formation by electric discharges in dust devils. *Life Sciences and Space Research*, *22*, 125–136. https://doi.org/10.1016/j.lssr.2019.02.007

Mason, J., Patel, M., Holmes, J., Wolff, M., Alday, J., Streeter, P., et al. (2024). Climatology and diurnal variation of O_3 column abundances for 2.5 Mars years as measured by the NOMAD-UVIS spectrometer. *Journal of Geophysical Research*, *129*(4), e2023JE008270. https://doi.org/10.1029/2023JE008270

Montabone, L., Spiga, A., Kass, D. M., Kleinböhl, A., Forget, F., & Millour, E. (2020). Martian year 34 column dust climatology from Mars Climate Sounder observations: Reconstructed maps and model simulations. *Journal of Geophysical Research*, *125*(8), e2019JE006111. https://doi.org/10.1029/2019je006111

Montmessin, F., Korablev, O., Lefèvre, F., Bertaux, J.-L., Fedorova, A., Trokhimovskiy, A., et al. (2017). SPICAM on Mars express: A 10 year in-depth survey of the Martian atmosphere. *Icarus*, *297*, 195–216. https://doi.org/10.1016/j.icarus.2017.06.022

Montmessin, F., Korablev, O. I., Trokhimovskiy, A., Lefèvre, F., Fedorova, A. A., Baggio, L., et al. (2021). A stringent upper limit of 20 pptv for methane on Mars and constraints on its dispersion outside Gale crater. *Astronomy & Astrophysics*. https://doi.org/10.1051/0004-6361/202140389

Murchie, S. L., Mustard, J. F., Ehlmann, B. L., Milliken, R. E., Bishop, J. L., McKeown, N. K., et al. (2009). A synthesis of Martian aqueous mineralogy after 1 Mars year of observations from the Mars Reconnaissance Orbiter. *Journal of Geophysical Research*, *114*(E2). https://doi.org/10.1029/2009JE003342

NASA. (2017). NASA Planetary Data System node for MCS data [Dataset]. *NASA*. https://atmos.nmsu.edu/data_and_services/atmospheres_data/MARS/mcs.html

Neary, L., Daerden, F., Aoki, S., Whiteway, J., Clancy, R. T., Smith, M., et al. (2020). Explanation for the increase in high altitude water on Mars observed by NOMAD during the 2018 global dust storm. *Geophysical Research Letters*, *47*(7). https://doi.org/10.1029/2019gl084354

Olsen, K. S., Fedorova, A. A., Kass, D. M., Kleinböhl, A., Trokhimovskiy, A., Korablev, O. I., et al. (2024a). Data from relationships between HCl, H_2O, aerosols, and temperature in the Martian atmosphere: 2. Quantitative correlations [Dataset]. *Journal of Geophysical Research*, *129*. https://doi.org/10.5287/ora-qmrokgjmr

Olsen, K. S., Fedorova, A. A., Kass, D. M., Kleinböhl, A., Trokhimovskiy, A., Korablev, O. I., et al. (2024b). Relationships between HCl, H_2O, aerosols, and temperature in the Martian atmosphere: 1. Climatological outlook. *Journal of Geophysical Research*, *129*. https://doi.org/10.22541/au.170967775.59762440/v1

Olsen, K. S., Fedorova, A. A., Trokhimovskiy, A., Montmessin, F., Lefèvre, F., Korablev, O., et al. (2022). Seasonal changes in the vertical structure of ozone in the Martian lower atmosphere and its relationship to water vapor. *Journal of Geophysical Research: Planets*, *127*(10), e2022JE007213. https://doi.org/10.1029/2022je007213

Olsen, K. S., Forget, F., Madeleine, J.-B., Szantai, A., Audouard, J., Geminale, A., et al. (2021). Retrieval of the water ice column and physical properties of water-ice clouds in the Martian atmosphere using the OMEGA imaging spectrometer. *Icarus*, *353*, 113229. https://doi.org/10.1016/j.icarus.2019.03.006

Olsen, K. S., Lefèvre, F., Montmessin, F., Trokhimovskiy, A., Baggio, L., Fedorova, A., et al. (2020). First detection of ozone in the mid-infrared at Mars: Implications for methane detection. *Astronomy & Astrophysics*, *639*, A141. https://doi.org/10.1051/0004-6361/202038125

Olsen, K. S., Trokhimovskiy, A., Montabone, L., Fedorova, A. A., Luginin, M., Lefèvre, F., et al. (2021). Seasonal reappearance of HCl in the atmosphere of Mars during the Mars year 35 dusty season. *Astronomy & Astrophysics*, *647*, A161. https://doi.org/10.1051/0004-6361/202140329

Ooki, A., & Uematsu, M. (2005). Chemical interactions between mineral dust particles and acid gases during Asian dust events. *Journal of Geophysical Research*, *110*(D3). https://doi.org/10.1029/2004jd004737

Osterloo, M. M., Anderson, F. S., Hamilton, V. E., & Hynek, B. M. (2010). Geologic context of proposed chloride-bearing materials on Mars. *Journal of Geophysical Research*, *115*(E10). https://doi.org/10.1029/2010JE003613

Osterloo, M. M., Hamilton, V. E., Bandfield, J. L., Glotch, T. D., Baldridge, A. M., Christensen, P. R., et al. (2008). Chloride-bearing materials in the southern highlands of Mars. *Science*, *319*(5870), 1651–1654. https://doi.org/10.1126/science.1150690

Patel, M. R., Sellers, G., Mason, J. P., Holmes, J. A., Brown, M. A. J., Lewis, S. R., et al. (2021). ExoMars TGO/NOMAD-UVIS vertical profiles of ozone: 1. Seasonal variation and comparison to water. *Journal of Geophysical Research*, *126*(11). https://doi.org/10.1029/2021je006837

Pollack, J. B., Colburn, D. S., Flasar, F. M., Kahn, R., Carlston, C. E., & Pidek, D. (1979). Properties and effects of dust particles suspended in the Martian atmosphere. *Journal of Geophysical Research*, *84*(B6), 2929–2945. https://doi.org/10.1029/jb084ib06p02929

Poncin, L., Kleinböhl, A., Kass, D. M., Clancy, R. T., Aoki, S., & Vandaele, A. C. (2022). Water vapor saturation and ice cloud occurrence in the atmosphere of Mars. *Planetary and Space Science*, *212*, 105390. https://doi.org/10.1016/j.pss.2021.105390

Quinn, R. C., Martucci, H. F. H., Miller, S. R., Bryson, C. E., Grunthaner, F. J., & Grunthaner, P. J. (2013). Perchlorate radiolysis on Mars and the origin of Martian soil reactivity. *Astrobiology*, *13*(6), 515–520. https://doi.org/10.1089/ast.2013.0999

Rajendran, K., Streeter, P., Duffy, M., Holmes, J., Lewis, S., Korablev, O., et al. (2024). Impacts of gas-phase chlorine chemistry and dynamical transport on the Martian surface perchlorate distribution. *Journal of Geophysical Research*, *129*.

Rao, B., Mohan, S., Neuber, A., & Jackson, W. A. (2012). Production of perchlorate by laboratory simulated lightning process. *Water, Air, and Soil Pollution*, *223*(1), 275–287. https://doi.org/10.1007/s11270-011-0857-y

Ruesch, O., Poulet, F., Vincendon, M., Bibring, J.-P., Carter, J., Erkeling, G., et al. (2012). Compositional investigation of the proposed chloride-bearing materials on Mars using near-infrared orbital data from OMEGA/MEx. *Journal of Geophysical Research*, *117*(E11). https://doi.org/10.1029/2012JE004108

Santiago-Materese, D. L., Iraci, L. T., Clapham, M. E., & Chuang, P. Y. (2018). Chlorine-containing salts as water ice nucleating particles on Mars. *Icarus*, *303*, 280–287. https://doi.org/10.1016/j.icarus.2017.11.001

Smith, M. D. (2004). Interannual variability in TES atmospheric observations of Mars during 1999-2003. *Icarus*, *167*(1), 148–165. https://doi.org/10.1016/j.icarus.2003.09.010

Smith, M. D. (2009). THEMIS observations of Mars aerosol optical depth from 2002-2008. *Icarus*, *202*(2), 444–452. https://doi.org/10.1016/j.icarus.2009.03.027

Smith, M. D., Pearl, J. C., Conrath, B. J., & Christensen, P. R. (2001). One Martian year of atmospheric observations by the thermal emission spectrometer. *Geophysical Research Letters*, *28*(22), 4263–4266. https://doi.org/10.1029/2001gl013608

Smith, M. L., Claire, M. W., Catling, D. C., & Zahnle, K. J. (2014). The formation of sulfate, nitrate and perchlorate salts in the Martian atmosphere. *Icarus*, *231*, 51–64. https://doi.org/10.1016/j.icarus.2013.11.031

Stevens, A. H., Patel, M. R., & Lewis, S. R. (2015). Numerical modelling of the transport of trace gases including methane in the subsurface of Mars. *Icarus*, *250*, 587–594. https://doi.org/10.1016/j.icarus.2014.12.033

Stevens, A. H., Patel, M. R., & Lewis, S. R. (2017). Modelled isotopic fractionation and transient diffusive release of methane from potential subsurface sources on Mars. *Icarus*, *281*, 240–247. https://doi.org/10.1016/j.icarus.2016.08.023

Streeter, P. M., Rajendran, K., Lewis, S. R., Patel, M. R., & Olsen, K. S. (2024). Impact of heterogeneous chlorine chemistry on Mars atmospheric hydrogen chloride. *Journal of Geophysical Research*.

Stremme, W., Grutter, M., Bayl'on, J., Taquet, N., Bezanilla, A., Plaza-Medina, E., et al. (2023). Direct solar FTIR measurements of CO_2 and HCl in the plume of Popocat'epetl Volcano, Mexico. *Frontiers in Earth Science*, *11*. https://doi.org/10.3389/feart.2023.1022976

Sullivan, R. C., Guazzotti, S. A., Sodeman, D. A., & Prather, K. A. (2007). Direct observations of the atmospheric processing of Asian mineral dust. *Atmospheric Chemistry and Physics*, *7*(5), 1213–1236. https://doi.org/10.5194/acp-7-1213-2007

Taysum, B. M., Palmer, P. I., Olsen, K. S., Luginin, M., Ignatiev, N., Trokhimovskiy, A., et al. (2024). Observed seasonal changes in Martian hydrogen chloride explained by heterogeneous chemistry on atmospheric dust and ice. *Astronomy & Astrophysics*. https://doi.org/10.1051/0004-6361/202449546

Thomas, N. H., Ehlmann, B. L., Meslin, P.-Y., Rapin, W., Anderson, D. E., Rivera-Hernández, F., et al. (2019). Mars science laboratory observations of chloride salts in Gale crater, Mars. *Geophysical Research Letters*, *46*(19), 10754–10763. https://doi.org/10.1029/2019GL082764

Tobo, Y., Zhang, D., Matsuki, A., & Iwasaka, Y. (2010). Asian dust particles converted into aqueous droplets under remote marine atmospheric conditions. *Proceedings of the National Academy of Sciences*, *107*(42), 17905–17910. https://doi.org/10.1073/pnas.1008235107

Villanueva, G. L., Mumma, M. J., Novak, R. E., Radeva, Y. L., Käufl, H., Smette, A., et al. (2013). A sensitive search for organics (CH_4, CH_3OH, H_2CO, C_2H_6, C_2H_2, C_2H_4), hydroperoxyl (HO_2), nitrogen compounds (N_2O, NH_3, HCN) and chlorine species (HCl, CH_3Cl) on Mars using ground-based high-resolution infrared spectroscopy. *Icarus*, *223*(1), 11–27. https://doi.org/10.1016/j.icarus.2012.11.013

von Glasow, R., & Crutzen, P. (2003). Tropospheric Halogen chemistry. In *Treatise on geochemistry* (pp. 1–67). Elsevier. https://doi.org/10.1016/b0-08-043751-6/04141-4

Wang, A., Jackson, A. W., Sturchio, N. C., Houghton, J., Yan, C. Y. C., Olsen, K. S., & Qu, Q. H. K. (2023). Quantification of Carbonates, oxychlorines, and chlorine generated by heterogeneous electrochemistry induced by Martian dust activity. *Geophysical Research Letters*, *50*(4). https://doi.org/10.1029/2022gl102127

Wang, A., Yan, Y., Jolliff, B. L., McLennan, S. M., Wang, K., Shi, E., & Farrell, W. M. (2020). Chlorine release from common chlorides by Martian dust activity. *Journal of Geophysical Research*, *125*(6). https://doi.org/10.1029/2019je006283

Wang, X., Jacob, D. J., Eastham, S. D., Sulprizio, M. P., Zhu, L., Chen, Q., et al. (2019). The role of chlorine in global tropospheric chemistry. *Atmospheric Chemistry and Physics*, *19*(6), 3981–4003. https://doi.org/10.5194/acp-19-3981-2019

Wilson, E. H., Atreya, S. K., Kaiser, R. I., & Mahaffy, P. R. (2016). Perchlorate formation on Mars through surface radiolysis-initiated atmospheric chemistry: A potential mechanism. *Journal of Geophysical Research*, *121*(8), 1472–1487. https://doi.org/10.1002/2016JE005078

Wray, J. J., Murchie, S. L., Squyres, S. W., Seelos, F. P., & Tornabene, L. L. (2009). Diverse aqueous environments on ancient Mars revealed in the southern highlands. *Geology*, *37*(11), 1043–1046. https://doi.org/10.1130/G30331A.1

Wu, Z., Wang, A., Farrell, W. M., Yan, Y., Wang, K., Houghton, J., & Jackson, A. W. (2018). Forming perchlorates on Mars through plasma chemistry during dust events. *Earth and Planetary Science Letters*, *504*, 94–105. https://doi.org/10.1016/j.epsl.2018.08.040